Palaeontologia Electronica
palaeo-electronica.org

Redescription of soft tissue preservation in the holotype of *Scaphognathus crassirostris* (Goldfuß, 1831) using reflectance transformation imaging

Nils Henkemeier, Kai R.K. Jäger, and P. Martin Sander

ABSTRACT

The description of the holotype of the non-pterodactyloid pterosaur *Scaphognathus crassirostris* from the Upper Jurassic Solnhofen Formation by the German palaeontologist Georg August Goldfuß in 1831 was the basis for the first published scientific life reconstruction of a pterosaur. In the time since Goldfuß, the technologies used in imaging soft parts in fossils have advanced greatly, but despite its historical importance, the holotype of *S. crassirostris* has received relatively little attention, limiting comparisons to more recent pterosaurian soft part finds. In this study, reflectance transformation imaging (RTI) was used to investigate fine surface details of the *S. crassirostris* type specimen. The observations of Goldfuß concerning the existence of different preservational patterns of the hair-like integumentary structures (pycnofibres) in this specimen were confirmed. Individual pycnofibre types differ both in their position and frequency and may indicate variation in pycnofibre morphology across different body regions in the living animal. Pycnofibre types forming a 'tuft' or a 'feather-like' structure are similar to those of other pterosaur fossils from the southern German Solnhofen Formation and the northeastern Chinese Tiaojishan Formation. However, some types, such as 'forked' pycnofibre impressions, could be artefacts of taphonomic processes. This study provides further evidence for the similarity in the preservation of integumentary appendages and associated preservational patterns in pterosaurs across different localities, palaeoenvironments, stratigraphic ages, and systematic positions.

Nils Henkemeier. Thüringer Landesmuseum Heidecksburg, 07407 Saalfeld, Germany. nils-henkemeier@t-online.de
P. Martin Sander. Abteilung Paläontologie, Institut für Geowissenschaften, Universität Bonn, Nussallee 8, 53115 Bonn, Germany. martin.sander@uni-bonn.de
Kai R.K. Jäger. Division of Paleontology, Steinmann Institute for Geology, Mineralogy, and Paleontology, University of Bonn, Nussallee 8, 53115 Bonn, Germany. jaegerk@uni-bonn.de

Key words: Pterosauria; Jurassic; soft tissue preservation; integument; imaging; palaeobiology

Final citation: Henkemeier, Nils, Jäger, Kai R.K., and Sander, P. Martin. 2023. Redescription of soft tissue preservation in the holotype of *Scaphognathus crassirostris* (Goldfuß, 1831) using reflectance transformation imaging. Palaeontologia Electronica, 26(2):a16. https://doi.org/10.26879/1070
palaeo-electronica.org/content/2023/3750-pterosaur-soft-parts

Submission: 17 February 2020. Acceptance: 4 January 2023.

INTRODUCTION

Pterosaurs were the first vertebrates in Earth's history capable of powered flight (Chatterjee and Templin, 2004; Elgin et al., 2011; Beardmore et al., 2017). They first appeared in the Late Triassic and were highly diverse, with substantial morphological disparity and taxonomic richness until the end of the Late Cretaceous (Benton and Pfretzschner, 2007; Longrich et al., 2018). Since their first scientific description in the late eighteenth century (Collini, 1784), pterosaur fossils have been known preserving not only hard parts (e.g., skeletal remains), but in extraordinary cases also soft parts that provide insights into their palaeobiology (e.g., Goldfuß, 1831; Zittel, 1882; Bennett, 2000, Tischlinger and Frey, 2002; Frey et al., 2003; Wellnhofer, 2008; Kellner et al., 2010; Witton, 2013). Although a variety of soft tissues are preserved in the pterosaur fossil record (including skin and internal organs), two types of soft parts appear to be unique to the group, warranting background discussion.

Soft Parts in Pterosaurs

Pycnofibres. Pycnofibres are filamentous structures in the integument of pterosaurs (Kellner et al., 2010). Pycnofibres were typically relatively short (five to seven millimetres in length), elongated structures that tapered towards the tip. They were of simple construction and, apart from a channel-like central hollow, do not seem to have had a complex internal structure (Witton, 2013). However, their appearance varied, and some pycnofibre types (at least in some taxa) seem to have been restricted to certain regions of the body (Yang et al., 2019). The fossil record suggests that pterosaurian pelage resembled that of densely-furred rather than more sparsely-haired mammalian taxa (compare Czerkas and Ji, 2002; Wang et al., 2002; Kellner et al., 2010; Witton, 2013). Pycnofibres may have been restricted to the body, including the tail, in most pterosaurs (Frey and Martill, 1998). However, they are also known from the distal area of the wing close to the wing finger and, at least in the case of the anurognathid *Jeholopterus ningchengensis* Wang et al., 2002 may have also been present on the wing surface itself, i.e., on the tenopatagium (Kellner et al., 2010).

It is unclear to what extent pycnofibres can be compared with the integumentary appendages of other vertebrates. It is generally assumed that the pterosaurian structures sometimes referred to as "hair" in the literature are not homologous with mammalian hair (Czerkas and Ji, 2002; Sträng, 2009). However, it is possible that the filamentous structures of pterosaurs and those of theropod dinosaurs may have had a common evolutionary root (Wellnhofer, 1975c; Czerkas and Ji, 2002; Witton, 2013; Yang et al., 2019). The alternative would be that pycnofibres appeared independently in pterosaurs, and thus are not causally related to the corresponding structures in theropods (Wellnhofer, 1975c; Tischlinger, 2006; Kellner et al., 2010) or ornithischians (Mayr et al., 2016). In the absence of early pterosauromorph and dinosauromorph fossils with well-preserved soft tissues, this relationship (i.e., the theoretical homology of pycnofibres with feathers) is likely to remain controversial (see Unwin and Martill, 2020; Yang et al., 2020).

Pycnofibres likely served a similar primary purpose to the integumentary appendages of extant tetrapods (e.g., hair): the regulation of the body temperature (Frey and Martill, 1998; Witton, 2013; Yang et al., 2019). As in extant taxa, however, these structures may have been multifunctional, with possible roles in tactile perception, improving flight characteristics, or signal function during courtship display (Wang et al., 2002; Yang et al., 2019).

Aktinofibrils and vessel structures. The second type of soft tissue structure unique to pterosaurs are aktinofibrils (Wellnhofer, 1987; Witton, 2013). The term "aktinofibrils" was first coined by Wellnhofer (1987), but their earliest scientific description goes back to Karl Alfred von Zittel (1882), who identified these structures in a specimen of the genus *Rhamphorhynchus* Meyer, 1846 (specimen number BSP 1880-II-8, the famous "Zittel wing").

The presence or absence of aktinofibrils distinguish two areas of the pterosaur wing (Kellner et al., 2010), with the proximal portion lacking them, but with the distal portion (aktinopatagium) showing a striking radiating pattern in a posterodistal direction (Schaller, 1985; Wellnhofer, 1987; Bennett, 2000; Tischlinger and Frey, 2002; Frey et al., 2003; Chatterjee and Templin, 2004; Kellner et al., 2010; Witton, 2013; Bennett, 2015; Hone et al., 2015). Aktinofibrils were densely packed in the wing (Kellner et al., 2010) and are hypothesised to

have increased the stability of the distal wing region despite their exceedingly small diameter (only 0.05-0.2 mm) (Wellnhofer, 1975c, 1987, 1991; Czerkas and Ji, 2002; Witton, 2013). Their spatial orientation within the wing membrane would have been variable depending on the respective wing position. In general, however, they were arranged approximately vertically relative to the bones of the forelimb and parallel to subparallel relative to the wing finger (Wellnhofer, 1987; Chatterjee and Templin, 2004; Kellner et al., 2010; Zhou and Schoch, 2011; Hone et al., 2015).

Individual aktinofibrils ran parallel to each other with a distance of ~0.2 mm to each other (Wellnhofer, 1975c, 1987; Tischlinger and Frey, 2002; Chatterjee and Templin, 2004). Their diameter and length do not seem to have remained constant within the wing membrane, as they decreased in the medial direction (Frey et al., 2003; Bennett, 2015). Aktinofibrils were probably rather rigid structures that maintained their length even when the wing was folded or stretched (Bennett, 2000; Witton, 2013). They were attached within a wedge of connective tissue to the wing finger (Witton, 2013; Bennett, 2015).

The function of aktinofibrils is less clear than that of pycnofibres and has been discussed extensively by pterosaur researchers (Padian and Rayner, 1993a, 1993b; Bennett, 2000; Bennett, 2015). While some authors considered a stabilising function of aktinofibrils to be plausible (Wellnhofer, 1975c, 1987; Chatterjee and Templin, 2004; Sträng, 2009; Kellner et al., 2010), Padian and Rayner (1993a) argued that aktinofibrils served to redistribute aerodynamic forces to the wing bones. Bennett (2000) interpreted the spatial arrangement of aktinofibrils within the wing membrane as an indication that their actual function was to relieve the distal phalanges by redistributing tensile forces to the proximal phalanges. Hence, aktinofibrils would have counteracted a narrowing of the patagium under tension. Finally, Tischlinger and Frey (2015) recently proposed that aktinofibrils played an important role in controlling fast flight manoeuvres, in interaction with the muscle layer contained within the patagium.

The position and composition of aktinofibrils have also been the subject of controversy. An external position of aktinofibrils on the outer surface of the wing membrane (i.e., an epidermal origin) would indicate a keratinous composition (Wellnhofer, 1991; Padian and Rayner, 1993a; Sträng et al., 2009; Bennett, 2015). However, the interpretation of aktinofibrils as external structures was opposed by Frey et al. (2003) and Kellner et al. (2010), who argued for an internal placement of the aktinofibrils within a flight membrane composed of several layers. If aktinofibrils were embedded in the wing membrane as internal structures, they likely would have consisted of collagen (Chatterjee and Templin, 2004).

Apart from pycnofibres and aktinofibrils, Solnhofen pterosaur fossils are also known to show remnants of other soft tissues. These are mainly vascular structures, the third relevant soft tissue type for the current study. One specimen of *Rhamphorhynchus* (JME SOS 4784) shows a rather complex network of vessels (Tischlinger and Frey, 2002; Frey et al., 2003). It has been assumed that this vessel system could have served as a transport system for air, blood, or lymphatic fluid (Frey et al., 2003, p. 244), but it may also have played an essential role in thermoregulation (Bennett, 2015). Based on recent models of the architecture of the patagium, such vascular systems are more likely to have been located on the ventral side of the patagium (see, for example, Tischlinger and Frey, 2015). Another notable soft tissue type known from Solnhofen pterosaurs is a connective tissue wedge along the posterior side of the wing finger, assumed to have played an important strengthening or aerodynamical role during flight (e.g., in the reduction of the drag) and probably made up of collagen fibres (Monninger et al., 2012).

Taphonomy of the Solnhofen Pterosaurs

The *Scaphognathus crassirostris* specimen examined here originates from the Solnhofen limestone deposits of the Franconian Alb, Bavaria. The fine-grained Solnhofen Formation deposits were deposited in basins, which are sometimes called “Wannen” in the German literature (Barthel, 1964, 1970; Keupp, 1993; Rauhut et al., 2017). These basins were not completely isolated from the surrounding sea, as the preserved fossils show both a terrestrial and a marine influence (Barthel et al., 1990). However, individual basins were largely protected from turbulent water flow by algae and sponge reefs. These circumstances allowed low-energy sedimentation conditions to develop (Barthel, 1964; Barthel et al., 1990; Kölbl-Ebert and Cooper, 2019).

Dead organisms (e.g., pterosaurs) were deposited at the bottom of the basins. This process was followed by the rapid coverage of the carcasses with sediment (Barthel et al., 1990). A reducing environment, low oxygen levels, a high salt content, and the scarcity of decomposers

favoured the delayed degradation of the organic matter and thus the excellent preservation of the fossils (Barthel, 1964; Barthel et al., 1990; Beardmore et al., 2017; Kölbl-Ebert and Cooper, 2019). Due to the limited amount of microbial activity, the outline of the body had the chance to be imprinted on the surrounding sediment; a prerequisite for the former soft tissues to be preserved as impressions (Barthel et al., 1990). Frey and Martill (1998) stated three essential factors involved in pterosaur soft part preservation: Firstly, the lithology of the sediment, which was particularly well-suited to reproduce the body shape in the Solnhofen Formation basins; secondly, the early diagenesis of the sediment, which also contributed to the high quality of the impressions; thirdly, the rapid precipitation of minerals replacing the former organic material.

Various types of soft tissues have been described from pterosaurs from the Solnhofen Formation. Though wing membranes (brachiopatagia), pycnofibres, and aktinofibrils have been known for a long time (Zittel, 1882; Wiman, 1925; Broili, 1927; Wellnhofer, 1975c, 1987; Barthel et al., 1990; Frey and Martill, 1998; Tischlinger and Frey, 2002; Frey et al., 2003; Tischlinger and Frey, 2013; Vidovic and Martill, 2014; Hone et al., 2015), other types of soft tissues have only been described relatively recently, such as cranial crests with internal fibres of varying orientation and skin impressions showing the anatomy of the foot (Bennett, 2002; Frey et al., 2003; Frey et al., 2011), e.g., webbed metatarsals and digits in the taxa *Rhamphorhynchus* and *Pterodactylus* Cuvier, 1809 (Frey et al., 2003). In one specimen of the latter genus, there are also fossilised heel and sole pads known. Furthermore, there is evidence for throat pouches in both genera (Frey and Martill, 1998; Frey et al., 2011; Vidovic and Martill, 2014).

Remnants of the brachiopatagium are best known in the genera *Scaphognathus, Rhamphorhynchus, Pterodactylus,* and *Anurognathus* Döderlein, 1923 (Frey et al., 2003). Two distinct modes of preservation are known for pterosaur patagia: 1. external moulds; 2. physical preservation, in which the former organic composition was lost and primarily substituted by phosphate minerals (Frey and Martill, 1998). Both modes of preservation occur in the Solnhofen Formation (Tischlinger and Frey, 2002; Frey et al., 2003).

Besides brachiopatagia, uropatagia and propatagia are also known in Solnhofen pterosaurs (Wellnhofer, 1975c, 1987; Frey and Martill, 1998; Tischlinger and Frey, 2002; Bennett, 2007; Vidovic and Martill, 2014). In the genus *Rhamphorhynchus*, there are also remains of a terminally located tail vane (Frey et al., 2003). Remains of the musculature or vascular system have also been reported, albeit rarely (Tischlinger and Frey, 2002; Frey et al., 2003; Bennett, 2007; Beardmore et al., 2017). In some cases, there is even evidence for the preservation of the original organic materials of soft tissues, i.e., in the form of ungual sheaths of claws (Frey et al., 2003).

Following the initial description of the integumentary structures later known as pycnofibres in the *Scaphognathus crassirostris* holotype (Goldfuß, 1831), they would not be reported again until the early twentieth century. The second pycnofibre record was in a specimen of the genus *Rhamphorhynchus* described by Wanderer (1908), although he was not aware of the exact nature of those soft tissues, and their identity was not confirmed until the redescription by Broili (1927). Only a few years later, the first report on a body coverage resembling fur in the genus *Pterodactylus* appeared (Broili, 1938; Frey et al., 2003). Apart from these, evidence exists for the presence of bristles in the cervical region in *Germanodactylus* Young, 1964 as well as in *Pterodactylus* among Solnhofen pterosaurs (Frey and Martill, 1998; Frey et al., 2003).

History of Research on the *Scaphognathus crassirostris* Holotype

One of the first scientifically founded life reconstructions of a pterosaur (and thus of an extinct vertebrate) can be traced back to Georg August Goldfuß (1782–1848; Tischlinger, 2003; Jäger et al., 2018). Goldfuß depicted his new pterosaurian taxon *Pterodactylus crassirostris* (later transferred to a new genus, *Scaphognathus* Wagner, 1861) in its presumed habitat, a steep coast by the sea (Goldfuß, 1831; plate 9; see also Figure 1). But Goldfuß also reconstructed the animal as having a fur-like body coverage. Therefore, Goldfuß has to be regarded as the first scientist having deliberated over the body coverage of pterosaurs (Tischlinger, 2003, 2006), and the holotype of *Scaphognathus crassirostris* represents the first record of pycnofibre preservation from the Solnhofen Formation (Frey et al., 2003; see Kellner et al., 2010 for an overview about pterosaurian soft parts). However, Herman von Meyer (1801–1869), one of the leading experts in the field of palaeoherpetology at that time, rejected Goldfuß's ideas (Frey et al., 2003; Tischlinger, 2003, 2006; Jäger et al., 2018), arguing that the supposed soft parts in this specimen were instead minerogenic precipita-

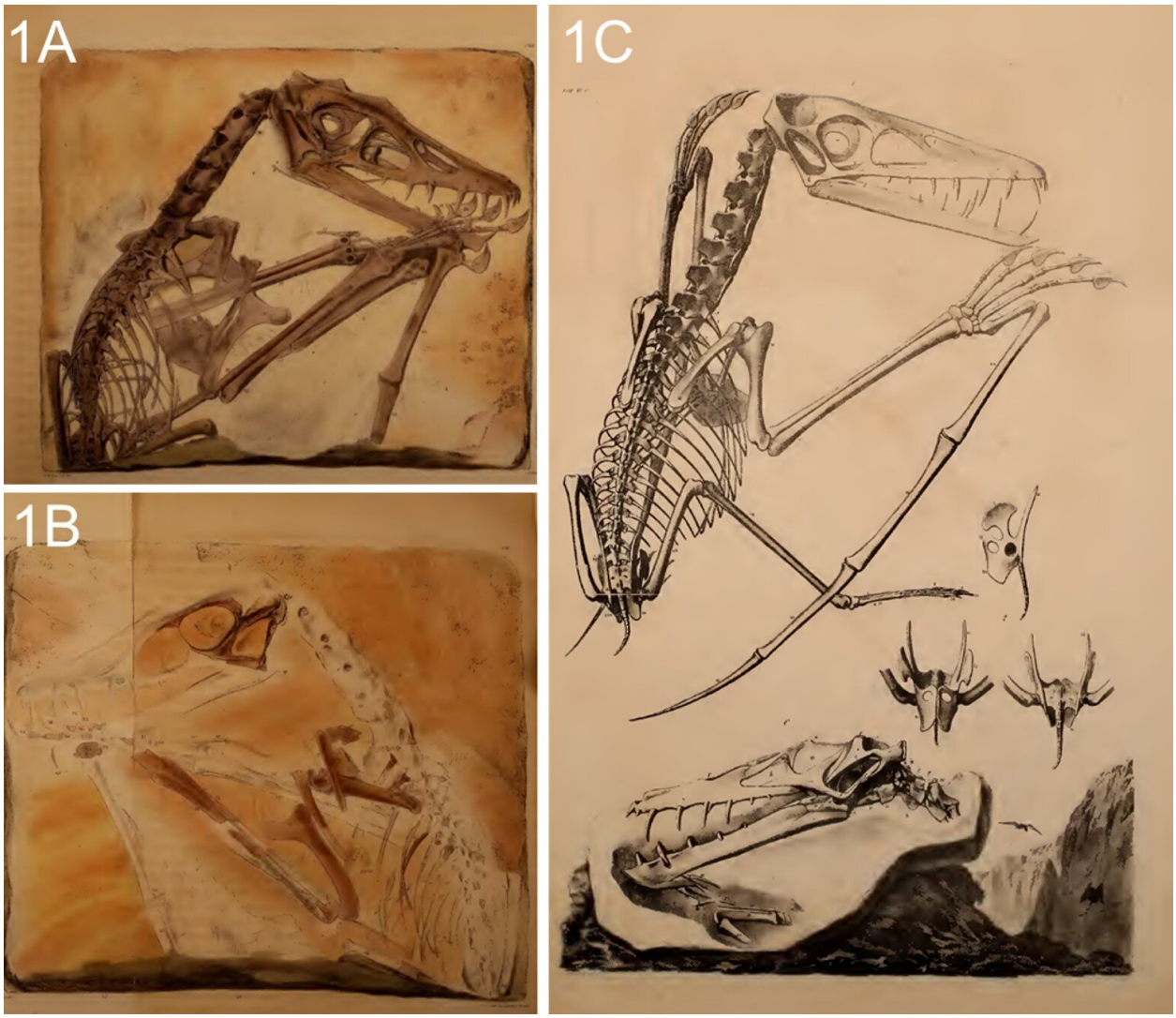

FIGURE 1. Images from the original publication by Georg August Goldfuß (1831). Main slab (1A) and counter slab (1B) of the holotype of *Scaphognathus crassirostris* IGPB Goldfuß 1304a (main slab) and 1304b (counter slab). 1C, Skeletal reconstruction of *Scaphognathus crassirostris*, including palaeobiological life reconstruction of two *Scaphognathus crassirostris* specimens in their presumed marginal marine habitat. However, the skeletal reconstruction contains two major errors: firstly, four instead of three clawed fingers are to be seen on the hand, and secondly, the long tail characteristic of most non-pterodactyloid pterosaurs is missing.

tions (Tischlinger, 2003; Jäger et al., 2018). Skepticism concerning the identification of soft parts in the *Scaphognathus crassirostris* continued through the twentieth century, as seen in Peter Wellnhofer's monographic works. For example, when summarising the genera from which parts of the wing membrane are known in his influential book, he did not mention the genus *Scaphognathus* at all (Wellnhofer, 1991, p. 149). Regarding the possible preservation of pycnofibres in the specimen, he noted that Goldfuß regarded them as impressions of tufts of hair, but did not agree with this interpretation, instead suggesting "in places somewhat wrinkled body skin" (Wellnhofer, 1975b, p. 179).

Therefore, the importance of Goldfuß's work was largely overlooked for much of the history of pterosaur palaeobiology, receiving a new appreciation only in the context of Helmut Tischlinger's investigations at the beginning of the twenty-first century. Tischlinger was able to verify the observations of Goldfuß using UV light (Tischlinger, 2003, 2006), confirming the existence of soft parts in all regions of the skeleton where Goldfuß believed them to be present. In addition to pycnofibre impressions, he was also able to document the phosphatically preserved aktinofibrils in the *Scaphognathus crassirostris* holotype for the first time (Tischlinger, 2003, 2006). Most recently, Jäger

et al. (2018) used reflectance transformation imaging (RTI) to study the specimen, corroborating and complementing the UV data. In particular, they noted that RTI provided better resolution of the preserved pycnofibres than previously used techniques and that this would be a useful avenue for future research. Here, we follow up on that, describing the preserved soft tissue of this specimen in detail. Apart from records of a few other genera, e.g., *Dorygnathus* Wagner, 1860 and the abundant, well-studied genus *Rhamphorhynchus*, the holotype of *Scaphognathus crassirostris* represents one of the few published finds within the family Rhamphorhynchidae known to show soft part preservation (Broili, 1939; Colbert, 1969; He et al., 1983; Carpenter et al., 2003; Gasparini et al., 2004; Andres et al., 2010; Lu et al., 2010; Lu et al., 2012; Cheng et al., 2012; Bennett, 2014; Zhou, 2014).

MATERIAL AND METHODS

Holotype of *Scaphognathus crassirostris*

The specimen (IGPB Goldfuß 1304a and b) investigated in this study is the holotype of the Upper Jurassic non-pterodactyloid pterosaur *Scaphognathus crassirostris* (Figures 1 and 2). It is in the collection of the Goldfuß-Museum, Section of Palaeontology, Institute of Geosciences of the Rheinische Friedrich-Wilhelms-Universität Bonn, Germany.

The specimen is preserved on two slabs of limestone, referred to as the main slab and the counter slab (Goldfuß, 1831; Jäger et al., 2018; see also Figure 1A-1B). The actual skeleton and the majority of soft part impressions lie on the main slab; there is no evidence of drag marks indicating the presence of the bones and soft tissue remains on the underlying counter slab (Viohl, 1990). On the counter slab, most bones are only visible as impressions (i.e., as whitish surfaces) and soft tissue impressions are much rarer than on the main slab. The skeleton lacks its posterior extremities and the distalmost part of the caudal vertebral column. Only the first phalanx and the proximal end of the second phalanx of the elongated right wing finger are preserved on the main slab.

Unfortunately, the exact circumstances of the find are unknown. The preservation is typical of the Solnhofen limestones, but the precise locality where it was found was not recorded. Goldfuß suspected that the specimen in question came from "the Jurassic formation of the Eichstädt area ..." (Goldfuß, 1831, p. 65). Since the holotype originates from the Solnhofen Formation, its age corresponds to the lowermost Tithonian (Upper Jurassic) (Barthel, 1964; Wellnhofer, 1975b).

Reflectance Transformation Imaging

General description of the technique. The usage of RTI in this study is a continuation of the research by Jäger et al. (2018), who also applied this method to the investigation of the holotype specimen. RTI files enable the user to analyse fine structures on the surface of an object by manipulating reflective properties and lighting conditions virtually (Malzbender et al., 2000; Hammer et al., 2002; Earl et al., 2010; Hammer and Spocova, 2013).

Thirty to 40 images were taken under varying illumination directions to create a polynomial texture map (Malzbender et al., 2000, 2001; Duffy, 2010; Cosentino, 2013). The raw images used are available at https://figshare.com under the following DOIs:

10.6084/m9.figshare.21809553;
10.6084/m9.figshare.21809577;
10.6084/m9.figshare.21809661;
10.6084/m9.figshare.21809688; and
10.6084/m9.figshare.21809706.

In this study, the "mobile highlight technique" was applied (see Jäger et al., 2018 for a detailed description of the technique). In contrast to the study of Jäger et al. (2018), much smaller black spheres with a diameter of 14 mm were used for the close-ups of regions with soft part preservation in the specimen. The distance of the movable flash functioning as the light source to the object was not measured exactly, as recommended by Jäger et al. (2018).

A total of six RTI files were created, four for the main slab and two for the counter slab. In total, these cover four different areas with soft tissue preservation: the area dorsal to the dorsal vertebral column until the base of the cervical vertebral column (1); the area ventral to the cervical vertebral column (2); the approximately triangular area dextral to the humerus of the right wing, which is enclosed by the bones of the zeugopodia (3); and the area ventral to the zeugopodial bones as well as left of the phalanges of the wing finger of the right wing (4) (Figure 2).

The software RTIViewer offers different rendering modes (Jäger et al., 2018). Within the scope of this study, the images were modified with the "specular enhancement mode" (Jäger et al., 2018). This mode helps to refine the shape of the object's surface, i.e., to improve the visualisation of the

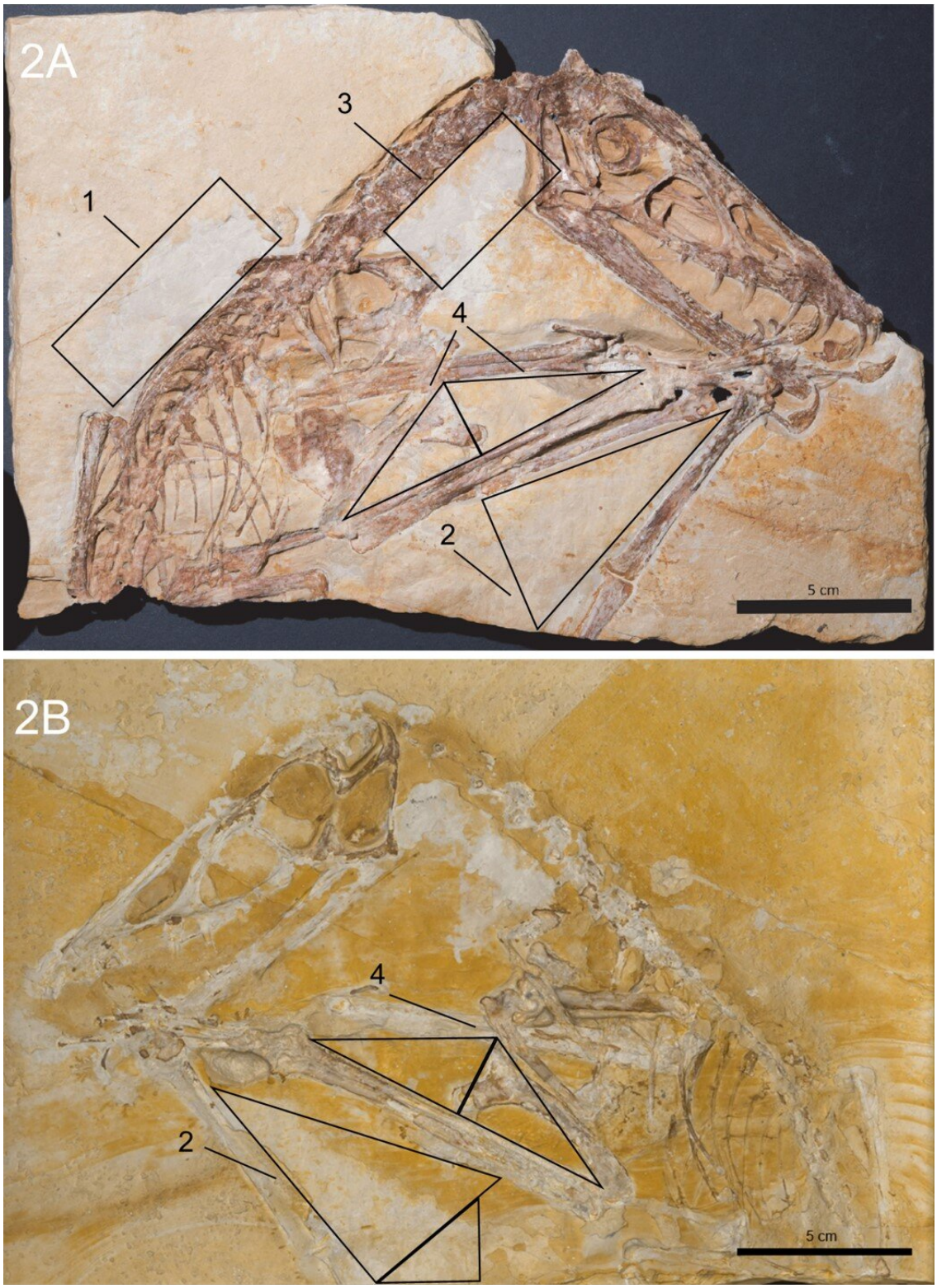

FIGURE 2. Main slab **(2A)** and counter slab **(2B)** of the *Scaphognathus crassirostris* holotype, IGPB Goldfuß 1304a and b. Black rectangles and triangles illustrate the four different body regions in which soft part preservation is present: dorsal to the dorsal vertebral column until the base of the cervical vertebral column (1), ventral to the zeugopodial bones and next to the first and second phalanx of the fourth wing finger of the right wing (2), ventral to the cervical vertebral column (3), and the region enclosed by the zeugopodial and stylopodial bones of both wings (4). Images adapted from Jäger et al. (2018).

topography (Malzbender et al., 2000, 2001; Hammer et al., 2002; Caine and Magen, 2011). It contains three different settings to vary the brightness of the image. The value of the setting "diffuse colour" was set to zero to create a whitening effect and to improve the visibility of the relief (Hammer and Spocova, 2013; Jäger et al., 2018). The values for "specularity" and the corresponding ones for "highlight size" were manipulated to provide ideal visibility. According to our own observations, the values for both parameters should be neither too high nor too low. To better accentuate the relief of the surface in the RTIViewer, relatively low-angled virtual light was chosen via the green light controller. In the following description of the soft tissue remains, images not processed with the specular enhancement mode are referred to as images studied under normal light. This notation also applies to text passages in which images are described whose areas were investigated only by a naked eye examination.

The description of the preserved soft tissues in the *Scaphognathus crassirostris* holotype is only based on the morphology of the structures itself, which results from a long taphonomical pathway to the present day. Therefore, note that the term "pycnofibre type" used here refers primarily to preservational patterns, recognising that these may not correspond precisely to anatomically distinguishable types of integumentary appendages found in the living animal. Several interpretations for the origin of these impressions are possible, which are discussed below.

Institutional Abbreviations

BSPG, Bayerische Staatssammlung für Paläontologie und Geologie, Munich, Germany; **CAGS**, Chinese Academy of Geological Sciences, Beijing, China; **ELTE**, Eötvös University, Budapest, Hungary; **IGPB**, Section of Paleontology, Institute of Geosciences, Rheinische Friedrich-Wilhelms-Universität Bonn, Germany; **IVPP**, Institute of Vertebrate Paleontology and Paleoanthropology, Beijing, China; **JME**, Jura-Museum, Eichstätt, Germany; **SNSD**, Senckenberg Naturhistorische Sammlungen Dresden, Germany.

RESULTS

Pycnofibres Dorsal to the Dorsal Vertebral Column

Soft tissue impressions and traces of preparation created by Goldfuß in 1829 or 1830 (personal obs. of archival materials) can be easily distinguished from each other: Smooth edges on the sediment surface near the bones (e.g., ventral to the zeugopodial bones of the right wing) indicate a careful removal of the sediment. It resulted in parallel striae underneath the preparation edge, which was smoothed out afterward (red arrow in Figure 3A). Thus, the colouration of a prepared surface near the bones appears rather homogeneous, whereas a sediment surface, which occurs together with soft tissues, still shows the original colouration (Donhauser, personal commun, 2019; green arrow in Figure 3A). While clearly visible on the main slab, pycnofibres are difficult to identify on the counter slab (Jäger et al., 2018; also personal obs.).

Pycnofibres are the most extensively preserved of all soft tissue types in the specimen. As noted by Goldfuß (1831), these are present as grooves on the main slab. In total, we recognised six distinct pycnofibre types preserved in the specimen on this slab. Only those impressions that allowed a more detailed description of their morphology, without being surrounded by overlapping/overlying impressions hiding the potential margins of the respective structures, were categorised as a type. Their complexity, including side branches and symmetry, clearly discriminates them from random distributions of neighbouring impressions and were, therefore, included in Table 1. In addition, the chosen pycnofibre types can be described without being greatly influenced by the reflective properties of the sediment surface resulting from the changing direction of the incident light. In most instances, the morphological description reflects the actual appearance of the impressions on the main and counter slab. In the few cases where length information is given, they only refer to the visible parts of the preserved structures. Thence, the description of the pycnofibre types given below represents an interpretation of the RTI images illustrated in Figures 4-11. In the following description of the soft tissue remains, the term "groove" is used for the pycnofibre impressions as well as for the organic remains between the zeugopodial bones of both wings on the main and counter slab. The term "indent", however, is used to describe an exceptionally large, curved, and whitish groove from which the more caudally located pycnofibres dorsal to the dorsal vertebral column originate (red arc in Figures 4C-4E and 5A-5C).

Dorsal to the dorsal vertebral column, pycnofibres occur in a high density. Their orientation and appearance differ depending on their position on the back (Figure 4A-4C). Pycnofibres in this area

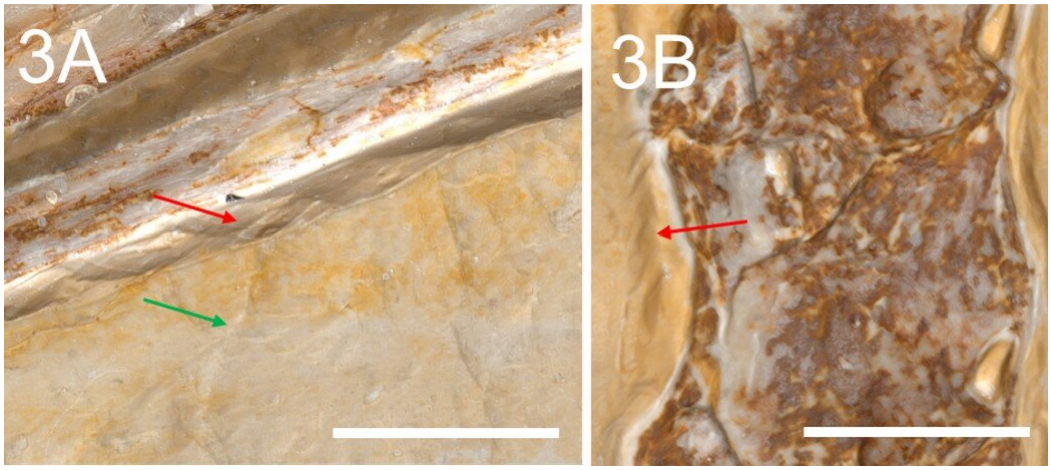

FIGURE 3. Close-ups of two different regions on the main slab demonstrating the optical difference between unprepared regions associated with soft parts (green arrow) and the surfaces prepared by Goldfuß (red arrow), without being processed with the specular enhancement mode. **3A.** The sharp border between the unprepared ochre- and beige-coloured limestone surface and the homogenous, striated surface directly ventral to the above-mentioned bones, which underwent preparation. **3B.** The striations created by Goldfuß are more clearly discernible dorsal to the cervical vertebral column (red arrow). Scale bar in both illustrations equals 10 mm.

are of variable length and curvature. Some impressions in the area of the anterior dorsal vertebrae appear to be relatively straight, with their tips curved only slightly caudally, towards the vertebral column. By contrast, the impressions in the more caudal direction dorsal to the dorsal vertebral column tend to be more strongly curved along the entire length of the corresponding pycnofibre impressions. Pycnofibre impressions dorsal to the dorsal vertebral column (and also ventral to the cervical vertebral column) are restricted to a distinct whitish amorphous surface made up of limestone. Many impressions in the caudal part dorsal to the dorsal vertebral column originate from the large indent mentioned above. From one curved end to the other, this indent measures almost 17 mm. Other whitish spots comparable to the one dorsal to the dorsal vertebral column are observable on the main slab, e.g., near the deltopectoral crest of the humerus (see Figure 2). Even though this whitish surface is full of pycnofibre impressions, it appears generally smoother than the surrounding ochre-coloured rock surface (Figure 4A).

In the more caudally oriented part of the dorsal indent (Figure 4A, 4C-4E), most pycnofibre impressions appear as elongated, curved, and largely unbranched grooves, which are arranged nearly parallel to each other. However, the RTI images also indicate at least one clearly intersecting or forked pycnofibre impression (Figure 4D, 4E). Most of the impressions in this area represent the first pycnofibre type, unbranched and oblong pycnofibres without further complexity (e.g., in the form of several side branches). The curved ends of the respective pycnofibres point away from the dorsal vertebral column towards the direction of the rock matrix. In the more caudal area dorsal to the dorsal vertebral column, pycnofibres start from the arched, large indent mentioned above (marked with a red arc in Figures 4C-4E and 5A-5C). Under normal light, the dorsal indent can be seen as a prominent whitish structure (see especially the red arc in Figure 4A). Several overlapping pycnofibres can be seen in this area both in the RTI images and by the naked eye (compare Figure 4A with 4D, 4E).

Unlike the caudally oriented pycnofibres, pycnofibres positioned more cranially tend to be more inclined towards the dorsal vertebrae (Figure 5A-5B). The respective tips of these pycnofibre impressions point towards the anterior dorsal vertebrae and lie relatively subparallel to them (Figure 5A-5C). The different orientation of the tips of the respective pycnofibre impressions between the more cranially and the more caudally oriented parts of the whitish indent dorsal to the dorsal vertebral column can clearly be observed (red arrows in Figure 4C and red marked angles in Figure 5A).

Type 1 pycnofibre impressions consist of single, undivided structures and are found in all portions of the main and counter slab where pycnofibres are preserved. Type 2 pycnofibre impressions are characterised by a bifurcation giving them a roughly “Y”-shaped appearance (Figure

TABLE 1. Table of the characteristics of the different pycnofibre types.

Pycnofibre type	Occurrence	General characteristics	Abundance and special features	Examples of Figures
1st type: Simple-shaped impressions	• dorsal to the dorsal vertebral column • ventral to the zeugopodia of the right wing • ventral to the cervical vertebral column	• elongated, curved and largely unbranched • commonly intersections or overlaps • high variability of curvature and orientation depending on the body region	• high; the predominant type • insertion from a striking indent at the dorsal vertebral column • mane-like appearance dorsal to the dorsal vertebral column	Figures 4A, 4C, 5A, 5B, 7C, 8C, 9B,
2nd type: bifurcations	• anterior part of the dorsal vertebral column • ventral to the zeugopodia of the right wing near the metacarpo- phalangeal joint	• two side branches branching off from a longer main branch • very characteristic Y-shape	• at least two occurrences, maybe even a third one on the counter slab	Figures 5A, 5B, 6G, 8C, 8E
3rd type: trident	• ventral to the zeugopodial bones of the right wing • ventral to the cervical vertebral column?	• terminal bifurcation consisting of three different side branches • side branches • more or less of equal length	• rare, one certain occurrence and one potential	Figures 6A, 6C, 6D, 6F, 9B
4th type: main branch with caudally bent side branches	• ventral to the zeugopodia of the right wing	• at least one side with several side branches bent caudally • slightly different length of the side branches	• unique occurrence • unusual symmetry with the side branches only at one side of the main branch	Figure 6D, 6F
5th type: tuft	• ventral to the zeugopodia of the right wing	• several side branches spreading out in a radiating pattern from a common starting point • decreasing length, but increasing curvature of the side branches towards the margin • middle side branch with a smaller bifurcation	• unique occurrence • possibly belonging to a much larger structure or even linked with the symmetrical feather (main branch of the feather)	Figures 6C, 6D, 6H, 7A
6th type: symmetrical feather	• ventral to the zeugopodia of the right wing at the articulation of the first with the second phalanx of the right wing finger	• two distinct parts: a terminal ramification consisting of several side branches and a main branch • variable length of the side branches with the length and curvature decreasing towards the centre of the ramification	• unique occurrence	Figure 7D, 7E, 7G, 7H

5A, 5B) and are to be found in the more caudal area dorsal to the dorsal vertebral column. Possible additional examples of this type are present ventral to the zeugopodia of the right wing (compare Figure 6D with 6G). However, the apparent forking in these could represent overlapping pycnofibres, as is the case elsewhere in this region (see Figure 5C).

In the cranialmost section of the whitish surface dorsal to the anterior dorsal vertebrae, anterior to the indent, pycnofibre impressions form slightly curved grooves running parallel to each other (Figure 5A-5C). In general, these impressions are less curved but are more regularly organised than those in the more caudal part above the dorsal vertebrae (Figures 4C and 5C). Impressions in this region do not have a uniform width or length but do indicate the presence of some fairly long pycnofibres (maximum length almost two centimetres), supporting Goldfuß's assumption of almost inch-long hairy pelage for the living animal (Goldfuß, 1831, p. 109).

Most pycnofibres dorsal to the first anterior dorsal vertebrae originate from a curved indent (red arc in Figure 5D-5F) similar in appearance to the indent in the more caudal region dorsal to the dorsal vertebrae. This indent is visible even under normal light (albeit only weakly) by using a magnifying glass. Goldfuß (1831) compared the appearance of pycnofibres in this area to "a fluffy, upwardly directed mane" (Goldfuß, 1831, p. 108: "…und auf der Hauptplatte zeigt sich auch auf der

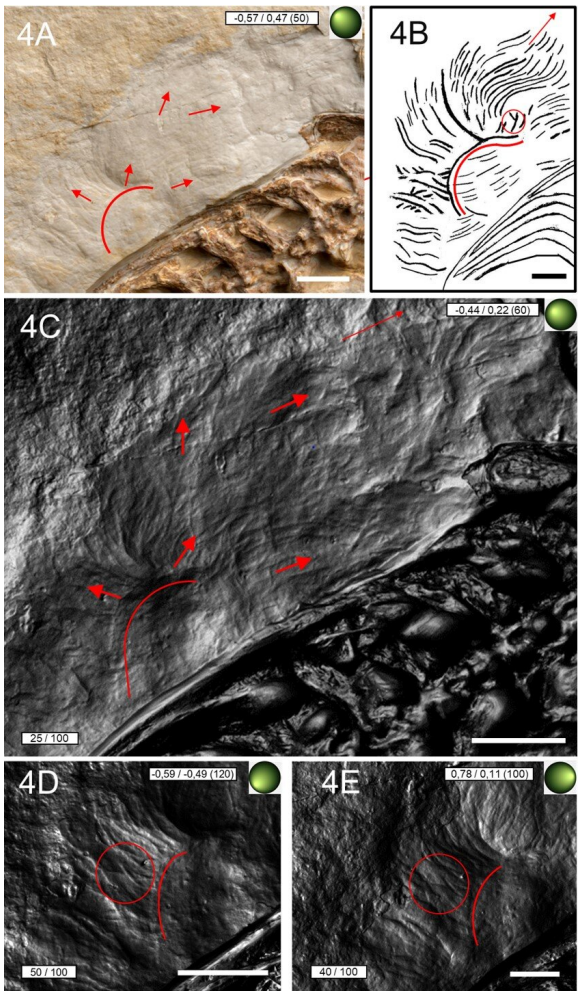

FIGURE 4. Close-up RTIViewer snapshots of the region dorsal to the dorsal vertebral column on the main slab, taken under different lighting conditions but all processed using the specular enhancement mode (except for Figure 4A). Scale bar for all illustrations equals 10 mm.

Comment on the settings in the RTIViewer software as visualised in the figures. A green sphere symbolises the direction of the incident light (upper right corner), a text box in the upper image margin contains the respective x- and y-coordinates of the incident light direction (the first value contains the x-coordinate, while the second one contains the y-coordinate), the zoom factor is given in brackets. A second text box contains the individual values of the specular enhancement mode (lower left corner). The first value stands for the parameter “specularity”, the second one indicates the parameter “highlight size”. The line drawings were sometimes made based on several RTI images with different settings to illustrate an individual impression more clearly. As far as the figures themselves are concerned, the interpretative drawings have tried to come as close as possible to the appearance and arrangement of the structures observed in the RTIViewer. However, some drawings, such as Figure 4B, represent rather idealised illustrations of the general pattern and arrangement of individual pycnofibre impressions in a given area. For this reason, the interpretative drawings may differ in detail from the respective RTI images to which they refer. In all figures, the orientation of the pycnofibres is marked by red arrows; the whitish semicircular indent, the starting point of most of the pycnofibres in the caudal region of the dorsal vertebrae, is symbolised by a red arc throughout Figure 4 and 5, the single occurrence of Type 2 pycnofibres is circled in red in the aforementioned figures.

4A. Overview of the pycnofibre impressions in the area dorsal to the dorsal vertebral column associated with the whitish amorphous rock surface under normal light. **4B.** Interpretative drawing of Figure 4A (dorsal ribs in the lower right corner of the image) under normal light, idealised to give an overview of the spatial orientation of the pycnofibre impressions and therefore not reflecting the exact path of individual impressions. Thicker lines indicate better observable impressions. **4C.** The same area as in 4A, seen under the specular enhancement mode. **4D.** Pycnofibres of the caudalmost part of the area dorsal to the dorsal vertebral column (lower right corner). Note the pycnofibres showing a distinctive cross-over (red circle in 4D and 4E), representing Type 2. **4E.** The same area as in 4D under other lighting conditions to highlight the overlapping impressions.

weissen [sic!] Stelle am Rücken der Abdruck einer flockigen, emporgerichteten Mähne…"). The RTI images demonstrate that the individual impressions spread out in a fan-like manner to all sides (see Figure 5D-5F). Some of these pycnofibre tips appear to be forked (orange circle in Figure 5D-5F).

Area Ventral to the Zeugopodium of the Right Wing and the Phalanges of the Right Wing Finger

Ventral to the zeugopodium of the right wing, near the phalanges of the right wing finger, pycnofibres are also common (Figure 6A, 6C). Pycnofibre impressions in this area are generally more abundant than the ones dorsal to the dorsal vertebral column, although less organised, based on the much higher number of overlying or crossed impressions, which complicates the identification of individual pycnofibre outlines. There is no consistent orientation of the individual pycnofibre impressions on this part of the slab, unlike the upwardly directed "mane" formed by impressions dorsal to the dorsal vertebral column (compare the differently oriented red arrows in Figure 4C with Figure 6A and 6C). The distinct whitish rock surface seen in the area dorsal to the dorsal vertebral column is absent ventral to the zeugopodium (Figure 6A). When this region is exposed to low-angled light without using the specular enhancement mode, pycnofibres are partly visible as distinctive grooves of variable length and orientation (Figure 6A).

Pycnofibres close to the articulation between the metacarpals and the phalanges of the right wing finger follow a pattern in which some pycnofibre ends point sub-parallel to each other and away from the zeugopodial bones (Figure 6A-6B and 6D-6E). The pycnofibre impressions in this area have a simple appearance: unbranched and curved, sometimes in a wave-like series. These unbranched pycnofibre impressions, although partly hard to see, are likely to be of the first type. The RTI images indicate that some of these pycnofibres cross or overlay each other, making separating individual filaments difficult, especially under normal light (Figure 6A).

Some pycnofibre impressions, comparable to those dorsal to the dorsal vertebral column, appear to have conspicuous forks and side branches pointing caudally (Figure 6D-6F). There is even one distinctive pycnofibre impression, which is characterised by a clear bifurcation resulting in two side branches forming a "Y" in shape (Figure 6B-6D and 6F-6G). It corresponds closely to the bifurcated pycnofibre impression dorsal to the dorsal vertebral column (Figure 5A-5B) and is classified as Type 2. Therefore, forked pycnofibres may be present in at least two different body regions of the *Scaphognathus crassirostris* holotype on the main slab: dorsal to the dorsal vertebral column and ventral to the zeugopodia of the right wing near the articulation of the metacarpal bone with the first phalanx of the right wing. These bifurcations are only clearly visible in the RTI images.

In addition to the simple "Y"-shaped impressions, an elongated, crooked pycnofibre is present with an even more pronounced bifurcation. It is located near the "Y"-shaped impressions, close to the articulation of the metacarpal bone with the phalanges of the right wing finger (Figure 6D-6F). This impression has several side branches of variable length and orientation, suggesting that it resulted from several individual filaments preserved together rather than an irregularly complex original pycnofibre type.

Two other important pycnofibre impression types are worth mentioning that are located close to those previously described. The first of these (Type 3) is located more distally in comparison to the second type shown in Figure 6G and is notable for being remarkably similar in shape to a trident (Figure 6C-6E). Its terminal portion consists of three side branches, which are more or less of equal length. The middle of these side branches has practically no curvature, whereas the outer ones are distinctly curved. All three point in the direction of the articulation of the metacarpal bone with the first phalanx of the right wing finger. The curvature of the outer side branch, which faces the zeugopodial bones, shows an even curvature, but the other, more distally located one, is characterised by a pronounced kink (Figure 6D and 6F). This morphology may be the result of a taphonomically influenced amalgamation of several individual impressions, especially since the most distally located side branch, which is itself curved, does not seem to have a direct connection to the remaining branching. Additionally, this impression type was only perceptible by using the specular enhancement mode. Nevertheless, this pycnofibre impression is distinguishable enough from all other branched structures described so far that it can be counted as an independent type. However, a trident-shaped pycnofibre is not unlikely to have once existed in the living animal, considering reports on branched integumentary structures in other pterosaurs with even more remarkable morphologies (see Yang et al., 2019). Moreover, the trident shape is only influenced to a lesser degree by

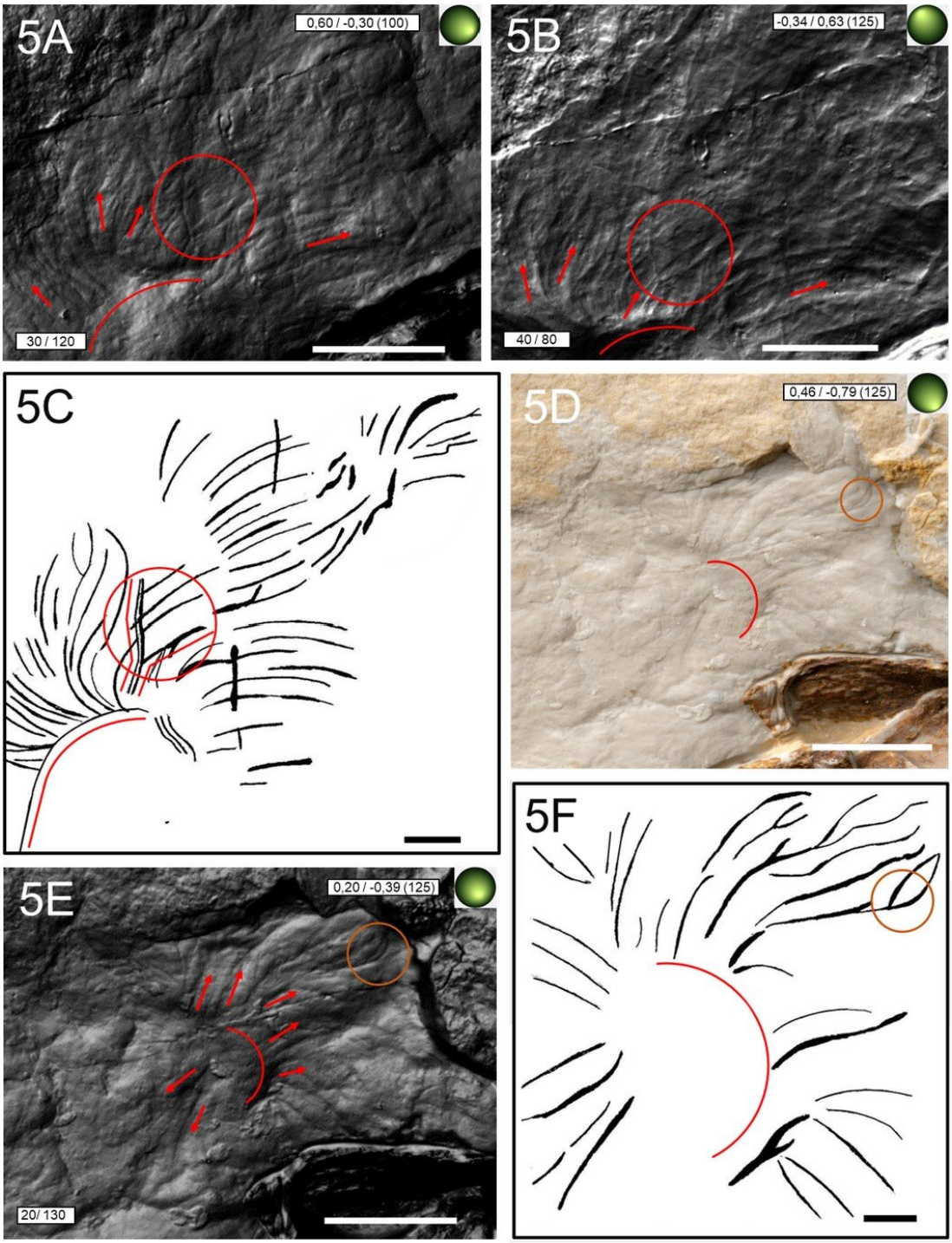

FIGURE 5. Close-up RTIViewer snapshots of the region dorsal to the dorsal vertebral column on the main slab, taken under different lighting conditions, but all processed using the specular enhancement mode (except for Figure 5D). Scale bar for all illustrations equals 10 mm. **5A-5B.** Caudal region dorsal to the dorsal vertebral column (lower right corner of both images) and next to the semi-circular indent, illustrated under different lighting conditions. **5C.** Sketch of Figure 5A and 5B showing the appearance and the orientation of the pycnofibres under normal light. **5D-5E.** Pycnofibres dorsal to the first anterior dorsal vertebrae (lower right corner), showing a striking pycnofibre accumulation under normal light (5D) as well as under the specular enhancement mode (5E). Note the spreading of pycnofibres in a radially symmetrical pattern from an arc-like starting point (red arrows, starting point marked by a red arc in 5E-5F). Also, note the branching in the dorsalmost part of the whitish limestone surface (orange circle in 5D-5F). **5F.** Interpretative drawing of 5D and 5E, illustrating the arrangement of the pycnofibre impressions under normal light.

the direction of the incident light, suggesting that this is also indeed an original pycnofibre type.

Type 4 pycnofibre impressions resemble those of Type 1 (unbranched, curving pycnofibre impressions; see Table 1), but with an important difference: at least one side, i.e., the side directed towards the metacarpal-phalangeal joint, shows at least three caudally curved side branches, with the possibility of a fourth (Figure 6B, 6D-6F). The main groove of type 4 impressions can be observed even with the naked eye, but its side branches are difficult to see without the RTI images.

In the direction of the elbow joint of the right wing, immediately ventral to the zeugopodial bones, an additional pycnofibre impression type (Type 5) is located at the edge of the unprepared sediment surface. This type is characterised by a tuft-like appearance (Figure 6H). The appearance of this tuft differs from that of the pycnofibre cluster dorsal to the dorsal vertebral column near the base of the cervical vertebrae (Figure 5C-5F). Seven side branches spread out in a radiating pattern from a common starting point, with their tips projecting towards the elbow joint. The tips of each of these side branches are curved, pointing in the same direction as the side branches themselves. In the middle section of the tuft, the longest of the side branches is split at its terminal part into two forks, with one running relatively straight, but with the other one showing the strongest curvature among the side branches (the region marked by the red circle in Figure 6H). The middle branch is also the longest of the side branches, which decrease in length towards the outer edges of the tuft. No other occurrences of a Type 5 impression could be identified in the specimen. The appearance of the tuft, i.e., its overall symmetry including the organisation of the side branches (i.e., the length difference between central and outer parts of the impression), remains constant regardless of the incident direction of light. This suggests that this structure is not a simple amalgamation of several individual impressions or the result of the reflective properties of the sediment surface (compare Figure 6C with 6H).

Perhaps it was this structure that Goldfuß (1831) described as “tufts”, in which one could identify a “more prominent, medium elevation”, from which “weaker elevations seem to diverge here and there” (Goldfuß, 1831, p. 108: “In den meisten Flocken unterscheidet man eine etwas stärker vorstehende, mittlere Erhabenheit, von welcher die andern schwachen hier und da zu divergiren [sic!] scheinen.”) Although the interpretative drawing Figure 7B suggests that the most distal side branches of the tuft may be continued in impressions that are curved and kinked to varying degrees and laying close to the tuft (see the red arrows in this drawing), it seems more reasonable to assume that the tuft represents a structure independent from adjacent impressions (see Figure 7A), especially since there are no direct connections between these side branches.

Exceptionally long, unbranched Type 1 pycnofibres are present distal to the second phalanx of the right wing finger at the edge of the main slab. Some of them are strongly curved (Figure 7C). In this region, the rock surface appears to be grooved, with the appearance of the individual pycnofibre impressions being variable depending on their curvature and with respect to their position towards the edge of the main slab. The degree to which these pycnofibre impressions show a straight versus curved shape also depends on their position in relation to the second phalanx of the right wing finger. In general, the degree of curvature of individual impressions decreases with increasing distance from the second phalanx (see red markings in Figure 7C). The shape of pycnofibre impressions located in the direct vicinity of the second phalanx and at the edge of the main slab can be described as either moderately or as strongly curved, whereas pycnofibre impressions located more distally from it are more or less straight in appearance (see Figure 7C).

To sum up, the above-mentioned pycnofibre impressions differ (slightly) in the spatial orientation of their tips from each other. Figure 7C (see red markings) illustrates that the curvature of pycnofibre impressions situated more proximal to the second phalanx of the right wing finger tend to be inclined in the direction of the relevant bone, whereas distally, some pycnofibre impressions point away from the second phalanx such that their tips are no longer facing the second phalanx, but lie subparallel to parallel to the bone. The described pycnofibre impressions intersect with each other and may even show forking in this region at the edge of the main slab. The impressions correspond to elevations of the same region on the counter slab (Figures 7C, 8C).

Dorsal to the articulation of the first and second phalanges of the right wing finger, there is a very distinctive accumulation of pycnofibre impressions, constituting an additional impression type of remarkable appearance (Type 6). These individual impressions branch off from a central main branch, which points towards the zeugopodial bones (Fig-

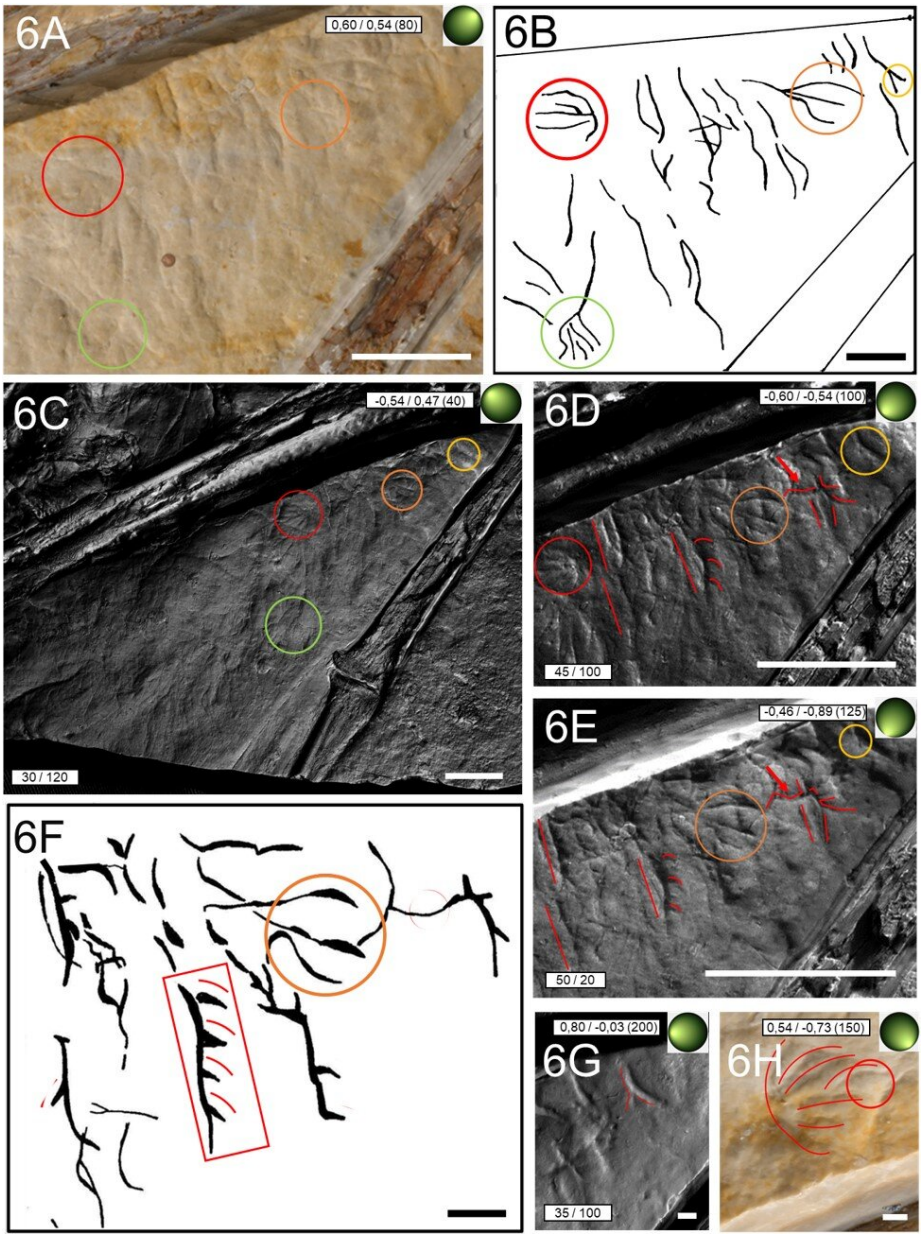

FIGURE 6. Close-ups of RTIViewer snapshots of the region ventral to the zeugopodial bones of the right wing on the main slab, taken under different lighting conditions, but all processed using the specular enhancement mode (except for 6A and 6H). Scale bar for all illustrations equals 10 mm, except for 6G and 6H (one millimetre). Markings for various pycnofibre types used throughout this Figure: Type 2 (bifurcated; yellow circle), Type 3 (trident-like; orange circle), Type 5 (tuft, red circle), and Type 6 (symmetrical "feather", green circle). The path of individual pycnofibre impressions, and the path of individual side branches of single impressions are illustrated by red markings (either by straight lines or by curved arcs as in 6D, 6E, and 6H). **6A, 6C.** Overview of the area with the pycnofibres ventral to the zeugopodial bones of the right wing (upper left corner of both images) and the phalanges of the right wing finger (near the right image margin) under normal light (6A) as well as under the specular enhancement mode (6C). **6B.** Schematic sketch of Figure 6C, showing the appearance of the pycnofibre impressions under normal light. **6D-6E.** Close-ups of 6C. Note the parallel to subparallel alignment of several pycnofibre impressions (red vertical lines in 6D and 6E) and the easily detected caudally curved side branches of the Type 4 pycnofibre (red rectangle in 6F). The complex structure with several putative side branches at the right image margin between Type 2 and 3 pycnofibres (red arrow) is more likely to represent an arrangement of overlapping impressions of individual pycnofibres. **6F.** Sketch of the RTI images 6D and 6E. **6G.** Detailed close-up of the Type 2 pycnofibre, outlined by red markings. **6H.** Detailed close-up of the Type 5 pycnofibre. The longest branch in the middle has a distinctive bifurcation (red circle).

ure 7D-7I). In the RTI images, this main branch appears to be a deeply embedded groove (Figure 7D and 7G). In the direction of the articulation of the first two phalanges of the right wing finger, the distal part of this main branch has impressions indicating side branches of variable length and degree of curvature. At this point, they occur in such a high density that their point of origin, the point where the central branch splits into several side branches, is referred to as a ramification.

Side branches closer to the center of the ramification are shorter than those further away and, in the RTI images, their curvature appears to be moderate, and are characterised by a distinct change of the direction towards the side. Their tapering tips are directed towards the remains of the patagium at the phalangeal articulation. Although the RTI images and their interpretation (compare Figure 7A-7B) seem to suggest a connection between impression Type 5 (the tuft, Figure 6H), and Type 6, the feather-like structure, there is no real evidence for a more complex pycnofibre type being composed of both types. As with the tuft, there is also no influence on the general arrangement and the length difference between the outer and more central parts of the ramification of the Type 6 impression, due to the changing direction of the incident light.

This structure might be what Goldfuß referred to as “the delicate, two-row diverging striation of a small bird feather” (Goldfuß, 1831, p. 109). As is the case for the Type 5, there is no indication of a comparable feather-like structure on the counter slab, nor are there other examples elsewhere on the main slab. This structure may be called a feather-like pycnofibre type, but it is highly unlikely that this impression, even if it is to be derived from a biological structure preserved without strong taphonomic influence, represents a true feather.

On the counter slab, the presence of pycnofibres can only be verified ventral to the zeugopodial bones of the right wing. Unlike the corresponding area on the main slab, pycnofibres on the counter slab are only visible in the region of a whitish amorphous rock surface (Figure 8A). In the lower part of the triangle formed by the phalanges and the zeugopodial bones of the right wing, pycnofibre impressions are mostly simple in shape (i.e., Type 1: unbranched and without any further complex morphology), elongated, and curved (Figure 8B-8D), except for one bifurcated pycnofibre (Figure 8E-8F). The bifurcated impression is similar to the forked pycnofibre (Type 2) dorsal to the dorsal vertebral column (compare Figure 5A-5B) and ventral to the zeugopodia of the right wing on the main slab (Figure 6G), but unlike the latter, the RTI image (red arrow in Figure 8E) suggests one side branch of the main bifurcation has a further, terminal bifurcation, much smaller than the main branch (yellow circle in Figure 8F). However, it remains unclear whether there is a real bifurcation of one of the main branches or not. There is also the possibility that there is only one real bifurcation with an adjacent impression overlapping one of the branches of the main bifurcation, resulting in the aforementioned smaller bifurcation.

The shapes of pycnofibre impressions on the counter slab cannot be determined with certainty via RTI because they change markedly depending on the direction of the incident light (compare Figure 8G, H with Figure 8I). This statement refers to the visible length, orientation, and position of the pycnofibres relative to each other in RTI. Unlike the pycnofibres at the lower edge of the counter slab, these pycnofibres appear to overlap in places (Figure 8G). Due to their unstable appearance in the RTI images, no reliable statement concerning their assignment to a particular type is possible.

Pycnofibres Ventral to the Cervical Vertebral Column

Few pycnofibres are observed ventral to the cervical vertebral column. They are mostly present in the triangle formed by the posterior end of the mandible and the anterior region of the cervical vertebrae (Figure 9A-9C). Similar to the dorsal region, a whitish, relatively smooth rock surface is present (Figure 9A). Under normal light and using a magnifying glass, pycnofibres appear as oblong, unbranched, and curved grooves (Type 1), similar to those dorsal to the dorsal vertebral column (compare for example Figures 4 and 5). On the main slab, ventral to the cervical vertebral column, only one pycnofibre impression is more complex. It appears to have a relatively symmetrical organisation of four side branches of equal length (interpretive drawing of Figure 9C). The side branches are similar in arrangement to the bifurcated Type 2 impressions (Figures 4 and 5), with the possible exception of two neighbouring bifurcations laying closely together (Figure 9B). These two supposed bifurcations are connected to each other by a long, somewhat S-shaped groove originating at the border between the unprepared and prepared sediment surface (see the oblong groove marked by the red arrow in Figure 9B and drawing Figure 9C). It is unclear to which type these bifurcations belong. Either these impressions could represent

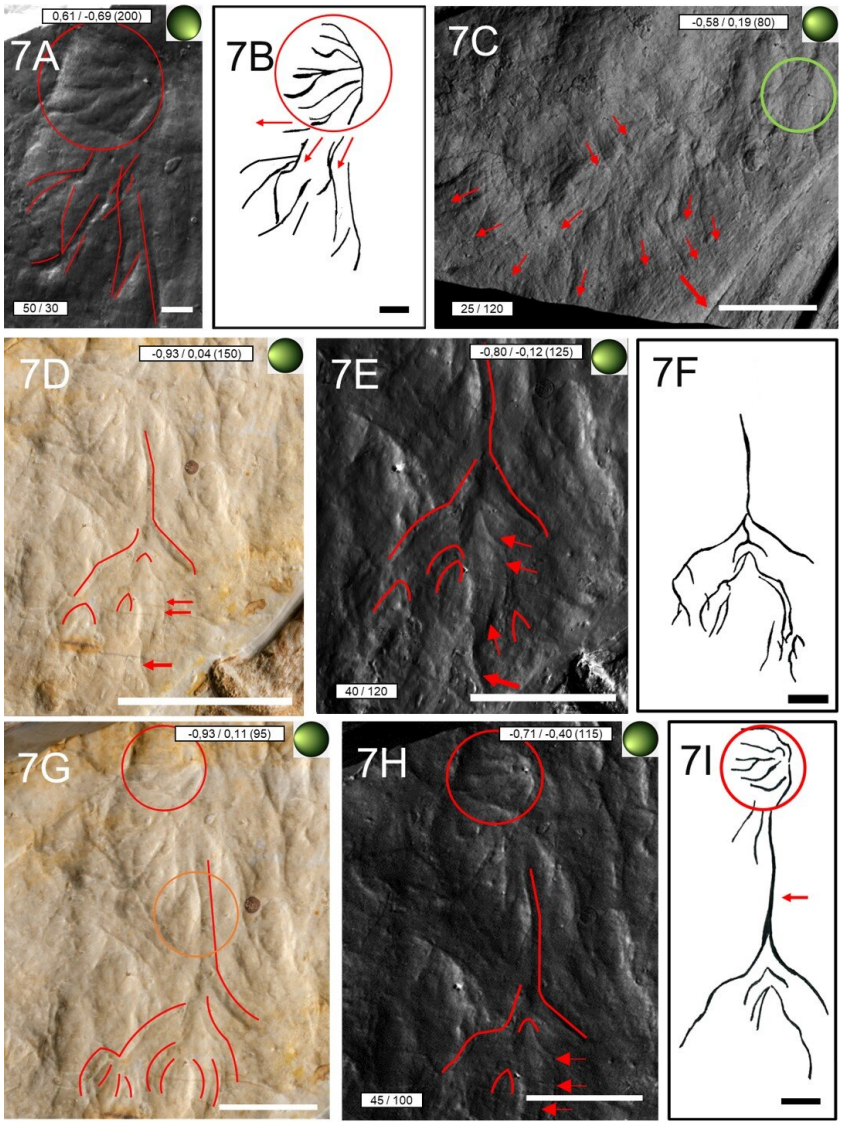

FIGURE 7. Close-ups of RTIViewer snapshots of the region ventral to the zeugopodial bones of the right wing on the main slab, taken under different lighting conditions, but all processed using the specular enhancement mode (except for 7D and 7G). Scale bar for all illustrations equals 10 mm, except for Figure 7A (1 mm). Markings for various pycnofibre types used throughout this figure: red circle illustrating Type 5 (the tuft); red arrows highlighting the main branch and several side branches of Type 6 (feather-like) as well as the individual path of single pycnofibre impressions at the lower margin of the main slab (Fig. 7C). For better comparability, the outermost (longest) side branches of the "feather" are highlighted by red markings (inclusive all terminal bifurcations). **7A.** Type 5 pycnofibre. Some impressions suggest a connection between the Type 5 and 6 pycnofibres, but are not consistent in their appearance. **7B.** Schematic drawing of Figure 7A, showing possible connections between the tuft and neighbouring grooves (see red arrows, although not entirely confirmable by the RTI images). **7C.** The accumulation of Type 1 pycnofibres at the edge of the main slab near the articulation of the first with the second phalanx of the right wing finger (towards the lower right corner). Red arrows indicate the opposing directions of the impressions. Note in the upper right image corner the sixth pycnofibre type of Figure 7D-7I (green circle). **7D.** Type 6 pycnofibre, dorsal to the articulation of the first with the second phalanx of the right wing finger (lower right image corner). Some side branches bear even smaller ones (red parabola-like upside-down markings in Figure 7D, 7E and 7H). **7E.** Specular enhancement image of the sixth type. **7F.** Interpretative sketch of 7E, highlighting the similarity with a feather as Goldfuß (1831) previously pointed out. The extent, length and number of several side branches are difficult to determine. Therefore, the drawing may differ in some details from the structure visible in the RTI images.**7G-7H.** The feather-like pycnofibre impression from a greater distance under normal light (7G) and processed by using the specular enhancement mode (7H). **7I.** Sketch of Figure 7G and 7H, suggesting no real connection between the Type 5 (tuft) and Type 6 (feather) pycnofibres.

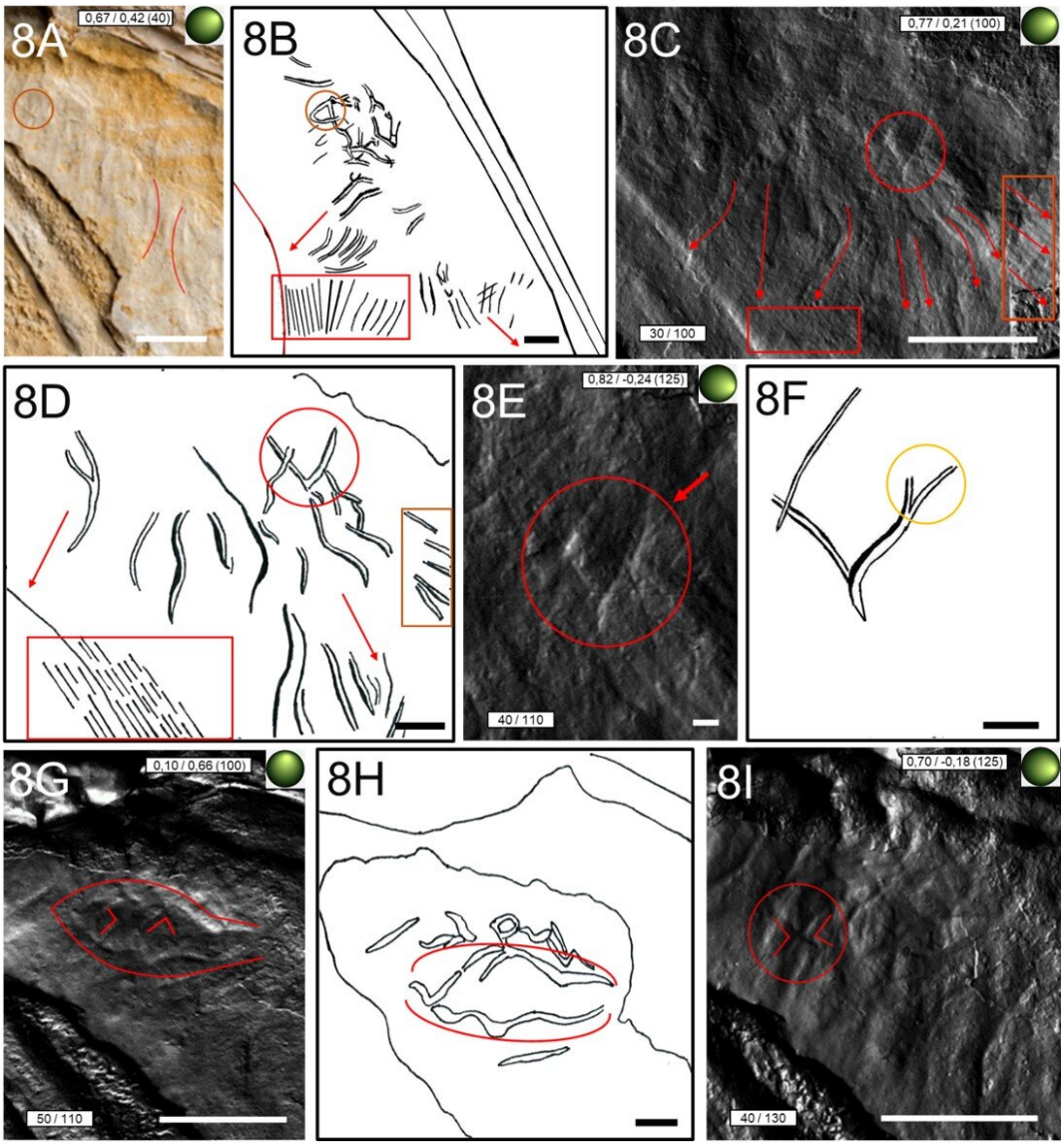

FIGURE 8. Close-up RTIViewer snapshots of the region ventral to the zeugopodial bones of the right wing on the counter slab, taken under different lighting conditions, but all processed using the specular enhancement mode (except for 8A). Scale bar for all illustrations equals 10 mm, except for 8E (1 mm). Markings for various pycnofibre types used throughout this Figure: the location of aktinofibrils impressions is marked by a red rectangle, the direction in which pycnofibre impressions point is highlighted by red arrows, the Type 2 pycnofibre is illustrated by a red circle. **8A.** The whitish amorphous rock surface with pycnofibres between the zeugopodial bones of the right wing (upper right corner) and the first two phalanges of the right wing finger (lower left corner). Note first type pycnofibre impressions (red lines). The locality of overlapping impressions is marked by an orange circle in 8A and 8B (although not well visible in the image). **8B.** Idealised sketch of Figure 8A after comparing several RTI images with each other to better visualise the trend of the decreasing abundance of crossing/ overlapping pycnofibres. Note that a trend of opposing impression directions seems to exist in this area of the counter slab (see the two red arrows). **8C.** Specular enhancement image depicting the lower image part of 8A encompassing a wider field of vision. Aktinofibrils-like impressions heading for the lower right edge of the image (red arrows within the orange rectangle). **8D.** Sketch of 8C. **8E.** Enlarged close-up of the Type 2 pycnofibre. A much smaller terminal bifurcation is indicated (red arrow), suggesting that it might even be another type of bifurcated pycnofibre. **8F.** Sketch of 8E, illustrating the smaller terminal bifurcation (yellow circle). **8G, 8I.** The inconsistent appearance of the pycnofibres directly ventral to the articulation of the metacarpal bones with the phalanges of the right wing finger, taking on interesting shapes depending on the direction of incident light (red oval in 8G and also indicated in 8H). At some places, the pycnofibre impressions cross each other at specific angles (marked by two red angles in 8G and 8I). **8H.** Sketch of 8G to highlight the oval shape of an accumulation of impressions.

two bifurcations of Type 2 pycnofibres next to each other (due to taphonomy), or they could belong to a type with a ramification made up of several side branches similar in appearance to Type 3 (Figure 6D-6F). However, since a definitive assignment is not possible, this accumulation of impressions is not counted as a further independent pycnofibre type.

Under normal light, signs of elongated, unbranched pycnofibres can also be seen ventral to the cervical vertebral column on the counter slab, meaning that they can also be classified as Type 1. It is notable that these impressions, analogous to the pycnofibres ventral to the zeugopodial bones of the right wing on the same slab, are also present on a whitish rock surface. However, the RTI images cannot confirm the existence of pycnofibres in this region, as previously noted by Jäger et al. (2018).

Aktinofibrils of the Aktinopatagium

On both slabs, aktinofibrils are present on the slightly whitish rock surface close to the first and second phalanx of the right wing finger, i.e., in the location of the aktinopatagium in the living animal (Bennett, 2000; Chatterjee and Templin, 2004; Kellner et al., 2010; see also Figure 9D and 9E). The aktinofibril impressions are only clearly observable with the help of a magnifying glass when studied under normal light by the naked eye. On the main slab, the appearance of aktinofibrils near the phalanges varies from sharply defined impressions to weaker, barely perceptible ones in the RTI images (Figure 9E). Also, in the RTI images showing the main slab, the most easily detectable aktinofibrils are found on an orange-brown sediment surface that is probably goethitic in origin. At the edge of the main slab, this sediment is limited to the area immediately dorsal to the phalanges of the right wing finger and a second, smaller spot further towards the knee joint of the right leg (Figure 9D). The arrangement of individual aktinofibrils impressions to each other is also seen outside of the prominent line which, according to Jäger et al. (2018), marks the border of the former aktinopatagium area (see Jäger et al., 2018). This line is to be found distal from the phalanges of the right wing finger and near the two orange-brown spots described before. The individual impressions of the aktinofibrils are straight, parallel to each other and parallel to subparallel to the wing finger (Figure 9D-9F).

Unlike the main slab, aktinofibrils on the counter slab are only visible distal to a prominent line that marks the edge of the aktinopatagium (Figure 8C-8D). Aktinofibrils impressions do not occur close to the impressions of the first and second phalanges of the right wing finger on the counter slab.

Organics Between the Zeugopodia of Both Wings

Soft tissue impressions in the triangle formed by the bones of the zeugopodia are distributed over two surfaces. One is bounded in the proximal direction by the elbow joint of the right wing and the deltopectoral crest of the right humerus. The other includes the more distal area from the deltopectoral crest of the right humerus to the point where the zeugopodial bones of both wings meet each other (see the two rectangles in Figure 10A).

On the main slab, several grooves are visible between the elbow joint and the deltopectoral crest of the humerus of the right wing. They extend over the whole sediment surface between the zeugopodial bones and the humerus of the right wing (Figure 10B-10E). These grooves vary in depth. In the RTI images, the appearance of the impressions varies depending on the direction of the incident light. The parallel organisation of some of the grooves near the zeugopodial bones is evident, while others are curved and approach each other (Figure 10C-10D).

These structures differ from pycnofibre impressions. They are not curved and lack crossings or intersections with other soft tissue impressions in the way that the pycnofibre impressions generally do and also lack the overall “hair-like” appearance of them (including the wavy-like looking pycnofibre impressions, such as the “mane” dorsal to the dorsal vertebral column, e.g., compare Figures 4C-4E and 5A-5B). Unlike the more irregular pycnofibre impressions, these structures are arranged at regular distances to each other, i.e., the overall appearance does not resemble a chaotic arrangement with overlapping and crossing impressions (red lines in Figure 10C-10E). They are organised in groups of three clusters, i.e., accumulations of soft tissue impressions with each cluster being characterised by having two or three individual impressions grouped together. Within each cluster, all individual impressions are oriented similarly to each other, but the orientation of individual impressions between different clusters varies (see line drawings in Figure 11A, 11C, and 11D). One cluster originates from a branch belonging to a central crossing located immediately proximal to the deltopectoral crest of the humerus, while

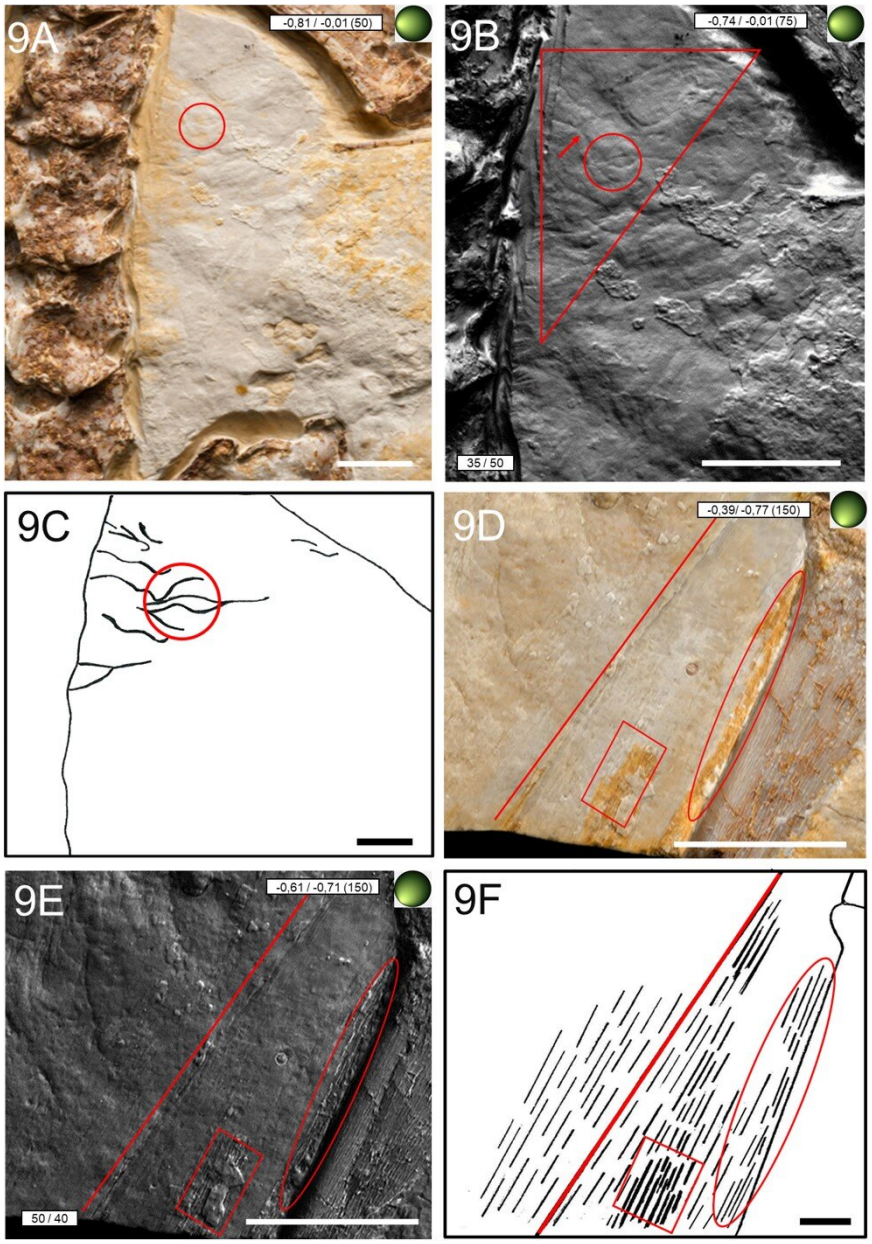

FIGURE 9. Close-ups of RTIViewer snapshots of the region ventral to the cervical vertebral column and at the articulation of the first with the second phalanx of the right wing finger on the main slab, processed without (9A and 9D) and with the specular enhancement mode (9B and 9E). Scale bar for all illustrations equals 10 mm. Markings for various pycnofibre types used throughout this Figure: The Type 2 (bifurcated) pycnofibre type is marked by a red rectangle, orange-brown sediment surfaces on which the aktinofibrils impressions are to be found are illustrated by a red rectangle and a red ellipse. The suggested border of the partly preserved wing membrane after Jäger et al. (2018) is also marked (red transversal line). **9A.** The whitish amorphous rock surface ventral to the cervical vertebral column. **9B.** Specular enhancement image of 9A. Frequent occurrence of pycnofibres marked by a red triangle. The pycnofibre accumulation within the red circle might represent closely spaced neighbouring bifurcated Type 2 pycnofibres (pointed out by a red arrow). **9C.** Interpretative drawing of 9B. **9D.** Aktinofibril impressions close to the articulation of the first with the second phalanx of the right wing finger, especially well preserved within two orange-brown sediment surfaces. Also note the presence of aktinofibrils on the surface of the phalanges, visible in 9D as well as in 9E (recognisable by a grooved bony surface). **9E.** Specular enhancement image of 9D. Aktinofibrils beyond the patagium border (and therefore laying on the bone surface of the phalanges) indicate their taphonomical displacement. **9F.** Interpretative drawing of 9E demonstrating the spatial arrangement of the aktinofibril impressions. Not shown are the aktinofibrils on the bone surface.

another branch spans the whole area between the deltopectoral crest of the humerus and the zeugopodia of the right wing.

In general, these soft tissues near (i.e., ventral) the deltopectoral crest of the humerus of the right wing have a much greater diameter compared to the pycnofibres, i.e., they appear thicker than the pycnofibre impressions in the RTI images. This refers above all to a prominent elevation approximately 11 mm away from the base of the deltopectoral crest of the right humerus, i.e., the longer branch of the central crossing mentioned above (Figure 11A-11C). The branches of the cross meet in such a way that they are almost at right angles to each other (see the cross in Figure 11C and 11D). Therefore, these structures are likely derived from some unknown soft tissue types originating from the former patagium, maybe some sort of a complex (blood) vessel system (see illustration caption of Figure 11A for a detailed discussion).

Another striking feature are channel-like grooves on the surface of the zeugopodial bones, appearing to be real indents that traverse the bone surface (see Figures 10 and 11). They have clearly marked margins. These channels are at places parallel aligned to each other. The appearance of individual channels varies between straight-lined but diagonally oriented grooves to grooves with very distinct, abrupt bends, which lead to a striking change of their course by 45º compared to their previous course. Although they present a chaotic appearance in places, individual grooves are connected by elongated channels, which run in the direction of the posterior-anterior axis of the zeugopodia. These channel-like grooves on the bone surface might have resulted from pathways for immigrating aqueous solutions precipitating iron minerals, resulting in the reddish-brown colouration of the bones.

On the counter slab, between the elbow joint and the deltopectoral crest of the humerus of the right wing, elongated elevations correspond to the aforementioned grooves found on the main slab (see Figure 10). Overlapping of individual elevations and their relative orientations are more easily recognisable on the counter slab (Figure 11A, 11C, 11D). The exact nature of these soft tissue structures on both the main and counter slab remains speculative, but they could be attributed to taphonomic derivations of a blood vessel layer, as described for the *Rhamphorhynchus* specimen JME SOS 4784 (Tischlinger and Frey, 2002).

Blood vessels are limited to the triangle between the deltopectoral crest of the humerus of the right wing and the intersection point of the respective zeugopodial bones of both wings (Figures 10A, 10F, 10G, and 11E-11G). They are elongated, slightly curved structures, arranged subparallel to each other (Figure 10F). They lack branches, except for the vessel located furthest distal to the humerus of the right wing, which has a bifurcation. However, this bifurcation is only apparent in the RTI images (Figure 10F) and especially on the counter slab (Figure 11E). The sediment surface with the blood vessels is interspersed relatively evenly with a high density of small, hole-like, rounded to elongated depressions on both slabs (Figures 10C-10D and 11E-11G) with a diameter of approximately 0.1-0.7 mm. Some of these are also present proximal to the deltopectoral crest of the humerus of the right wing. On both slabs, they occur in a relatively high density (12 individual pits per cm^2 in the region of the main slab illustrated in Figure 10G).

DISCUSSION

Comparison to the Observations of Goldfuß

With RTI, it was possible to verify the main observations of Goldfuß concerning soft part preservation in the *Scaphognathus crassirostris* holotype (supporting previous work by Jäger et al., 2018), as well as to recognise several novel integumentary impression types in the specimen (comparable to some forms seen in other pterosaurs; see, e.g., Wang et al., 2002; Kellner et al., 2010; Yang et al., 2019). In particular, these include complex pycnofibre impressions ventral to the zeugopodia of the right wing, here classified as Type 2 (Figures 5A, 5B, and 6G), Type 3 (Figure 6A, 6C- 6F), and Type 4 impressions (Figure 6B, 6D, and 6E).

Analogous to Jäger et al. (2018), the postulates of Goldfuß that soft part preservation is present in the holotype could thus be verified in almost all regions. For example, Goldfuß recognised the “white spot on the back” on the main slab and wrote of a possible body coverage composed of hairs or feathers. He compared these pycnofibre impressions with a “fluffy, upwardly directed mane” and concluded that the living animal was covered “not like the reptiles with scales and shields, but with a fur of soft, almost inch-long hair, perhaps in some places even with feathers” (Goldfuß, 1831, p. 108 f.: “Der *Pterodactylus crassirostris* war demnach nicht wie die Reptilien mit Schuppen und Schildern, sondern mit einem Pelz von weichen, fast Zoll langen Haaren , vielleicht an manchen Stellen sogar mit Federn bekleidet.”) The RTI

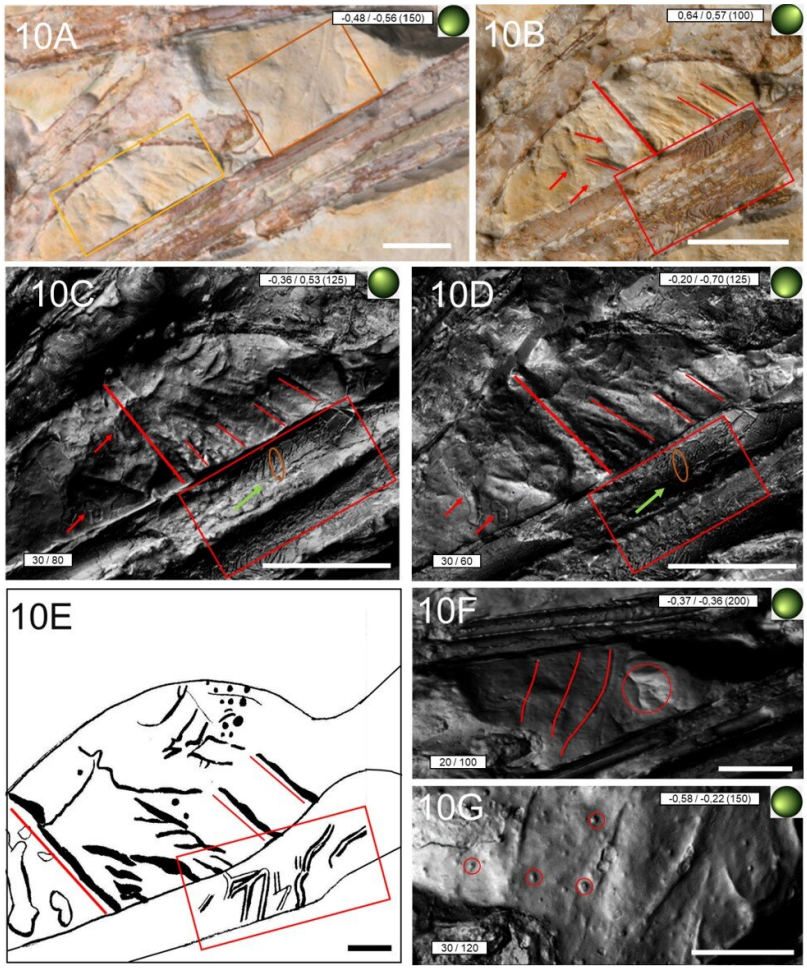

FIGURE 10. Close-up RTIViewer snapshots of the region enclosed by the articulation of the humerus with the zeugopodial bones of the right wing and the intersection point of the zeugopodial bones of both wings on the main slab, taken under different lighting conditions, but all processed using the specular enhancement mode (with the exception of 10A and 10B). Scale bar for all illustrations equals 10 mm. Markings for various soft part impressions used throughout this Figure: the longest soft part impression connecting the zeugopodial bones of the right wing with the humerus of the same wing is marked by a thick transversal red line, the other shorter ones running parallel to subparallel to each other by thin red lines, channel-like grooves on the bone surface are pointed out by a red rectangle. Dissolved limestone layer surfaces are pointed out by red rectangles. **10A.** Overview over the area with the organic remains between the zeugopodial bones of both wings. The location of the most pronounced grooves is highlighted (yellow rectangle) as well as the blood vessels (orange rectangle). Image modified from the .rti file of Jäger et al. (2018). **10B.** The impressions in this area do not share a common starting point. Note the parallel to subparallel arrangement of the shorter soft part impressions. Also, pay attention to the channel-like grooves on the bone surface and the whitish irregularly-shaped stains of the sediment layer between the zeugopodial bones, probably being the result of aqueous solutions, which might have occurred during fossilisation, and which might have dissolved the former uppermost sedimentary layer. Although speculative, such solutions might have been derived from escaping body fluids in the context of the taphonomy of the integumentary appendages (see Foth, 2012 for a detailed discussion). **10C-10D.** Specular enhancement images of 10B, taken under different lighting conditions to highlight the parallel arrangement of the soft part-related impressions and the channel-like grooves on the bones. Note the oblong channel connecting individual shorter ones (thick green arrow) and especially the zigzag pattern of some shorter channels (brown ellipse in both figures). **10E.** Interpretative drawing of Figure 10C and 10D. **10F.** The blood vessels near the intersection point of the zeugopodial bones of both wings. The subparallel alignment of the vessels (red slightly curved lines in Figure 10F) might indicate a similarity with the blood vessel system in the *Rhamphorhynchus* specimen JME SOS 4784 (Tischlinger and Frey, 2002; Frey et al., 2003). Note the distinct bifurcation of the rightmost vessel (red circle). Image modified from the .rti file of Jäger et al. (2018). **10G.** Detailed close-up of Figure 10F. Small pits (red circles) might be the result of degradation processes in the context of the decay of the pterosaur carcass, although the exact generic process is uncertain.

images also confirmed Goldfuß's skilled powers of observation, since all the different pycnofibre types mentioned in his publication of 1831 could be verified. Among the different pycnofibre types described in this study, the parallels between our own description and that of Goldfuß are most obvious in the case of Types 1, 5, and 6. In particular, the description of the 'fluff' by Goldfuß, in which a medium elevation (likely meaning a particularly well-developed side branch) spreads to a greater extent than the other elevations, brings to mind the Type 5 tuft (cf. Figure 6H).

However, there are also discrepancies between our findings and the observations of Goldfuß. This includes the position of individual soft tissue impressions on both slabs, their interpretations, and also the presence of soft tissue types that Goldfuß did not mention, e.g., the aktinofibrils (Figure 8D, 8E) or the blood vessels (Figures 10 and 11). Goldfuß also identified some pycnofibre impression types that were confirmed by this study, but in different locations than he indicated. A notable example is Type 6, the feather-like structure (Figure 7D-7I), which was observed by Goldfuß at a location near the right wing finger, where RTI could not detect any soft part preservation, only rock matrix (compare Goldfuß, 1831, plate 8, signature λ).

Some structures considered by Goldfuß to be remnants of soft tissues are inorganic formations, e.g., the reddish-brown stripes dorsal to the cervical vertebral column on the counter slab. Goldfuß also interpreted these striations as remains of integumentary appendages (Goldfuß, 1831, p. 109). However, these structures are instead discolourations of the rock surface, probably caused by Liesegang effects, as are known from other Solnhofen Formation fossils, e.g., *Compsognathus longipes* Wagner, 1859 (Reisdorf and Wuttke, 2012). Reisdorf and Wuttke (2012) concluded that the Liesegang marks in the *Compsognathus longipes* specimen BSPG AS I 563 are made up of iron hydroxide. The reddish colouration of the corresponding structures in the *Scaphognathus crassirostris* holotype suggests an identical mineralogical composition. Furthermore, Goldfuß noted "forward-directed hair tufts" close to the cervical vertebral column on the main slab (Goldfuß, 1831, p. 109). With RTI, however, no "tufts" could be identified in this area.

Critical Evaluation of RTI for the Use in the Analysis of Fossils

The RTI method offers some major advantages, but also disadvantages when it comes to the investigation of details on a sediment surface with exceptionally low relief, as is the case for this study. The most important advantages of RTI over conventional imaging techniques are the improved visualisation of three-dimensional surface structures and the consideration of reflective properties on the surface (Malzbender et al., 2000, 2001). Therefore, RTI increases the perceptibility of surface structures compared to photographs (Malzbender et al., 2001). For this reason, an RTI model represents a far more realistic representation of three-dimensional shapes on the surface, which improves the study of morphological details (Earl et al., 2010; MacDonald, 2011; Cosentino, 2013), including the perceptibility of surface details not documentable by a direct physical examination (MacDonald, 2011). This better visualisation of fine surface details is due to the lack of data loss caused by the presence of light and shadows in traditional imaging (Mudge et al., 2006). A disadvantage of RTI, however, is that the mobile highlight technique used in this study is susceptible to errors, as the correct arrangement of the light source cannot be checked virtually (Barbosa et al., 2007).

Rendering modes like the specular enhancement mode contained in the RTIViewer permitted the visualisation of the aktinofibrils and other structures that were not visible to Goldfuß. Another advantage of RTI is that the optimal illumination for the study of soft tissues and their visualisation in scientific illustrations can be set with little effort (Jäger et al., 2018). In contrast to the RTI method, regular photographic methods traditionally used in palaeontology illustrate the optical properties of an image, such as colour, reflection, or shading, only on a two-dimensional plane (Hammer et al., 2002). Unlike RTI, these methods often struggle to highlight small relief differences on low-relief fossils (Hammer et al., 2002; Béthoux et al., 2016).

A major disadvantage, however, was the unstable appearance of the pycnofibres under the varying directions of the incident light, often making it difficult to interpret their real appearance. Moreover, many pycnofibres overlap or cross each other, obscuring the outlines of individual pycnofibres even with RTI. This was the case, for example, with the pycnofibres on the counter slab (see Figure 8G and 8I). Therefore, future studies using RTI should compare the structures visible in the

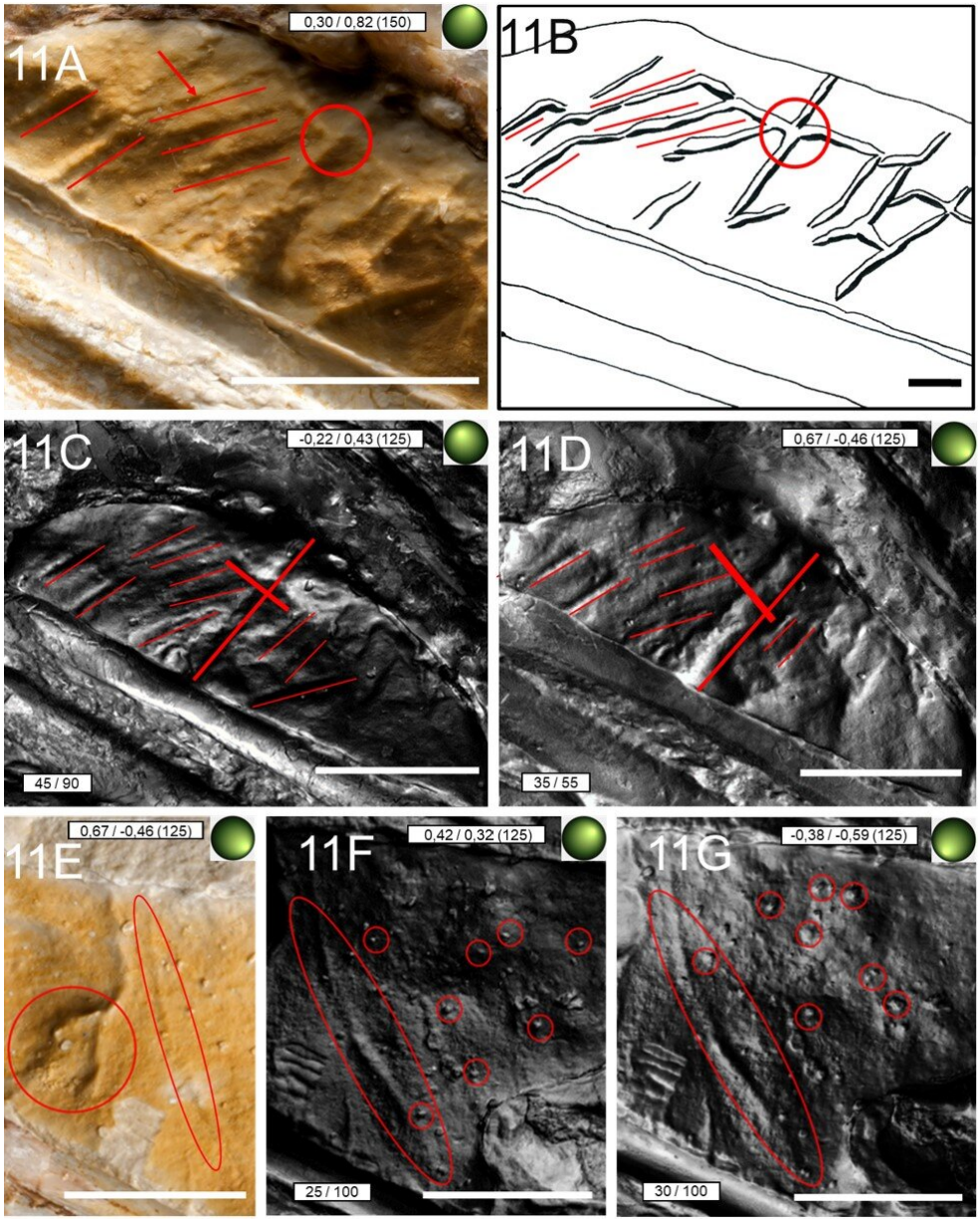

FIGURE 11. Close-up RTIViewer snapshots of the region enclosed by the articulation of the humerus with the zeugopodial bones of the right wing and the deltopectoral crest of the humerus on the counter slab, taken under different lighting conditions, but all processed using the specular enhancement mode (except 11A and 11E). Scale bar for all illustrations equals 10 mm. Markings for various soft part impressions used throughout this Figure: red lines illustrate the path of the impressions and their orientation to each other and a red ellipse marks the longest blood vessel. **11A.** The geometrically organised soft parts ventral to the deltopectoral crest of the humerus (uppermost left corner) and the zeugopodial bones of the right wing (lower margin). Note the distinct crossing of the two thick main branches (red circle in 11A and 11B). The arrangement of these impressions of a soft tissue type that cannot be determined with absolute certainty, but very probably once belonging to the Patagium reminds of the arrangement of the main vessels in the complex vessel system in the *Rhamphorhynchus* specimen JME SOS 4784 (Tischlinger and Frey, 2002; Frey et al., 2003). In this specimen, a large main vessel serves as an attachment point for side channels branching off from it at more or less right angles. **11B.** Interpretative drawing of 11A. **11C-11D.** Specular enhancement images of Figure 11A under different lighting conditions. The soft part impressions likely representing former patagium vessels appear either as elevations (11C) or as grooves (11D). The parallel arrangement of some side branches is confirmed under all lighting conditions, suggesting its interpretation as part of the patagium. **11E.** The longest, unbranched and strongly bifurcated blood vessel (red circle in 11E). **11F-11G.** The appearance of the pit-like depressions already shown in Figure 10 associated with the blood vessels.

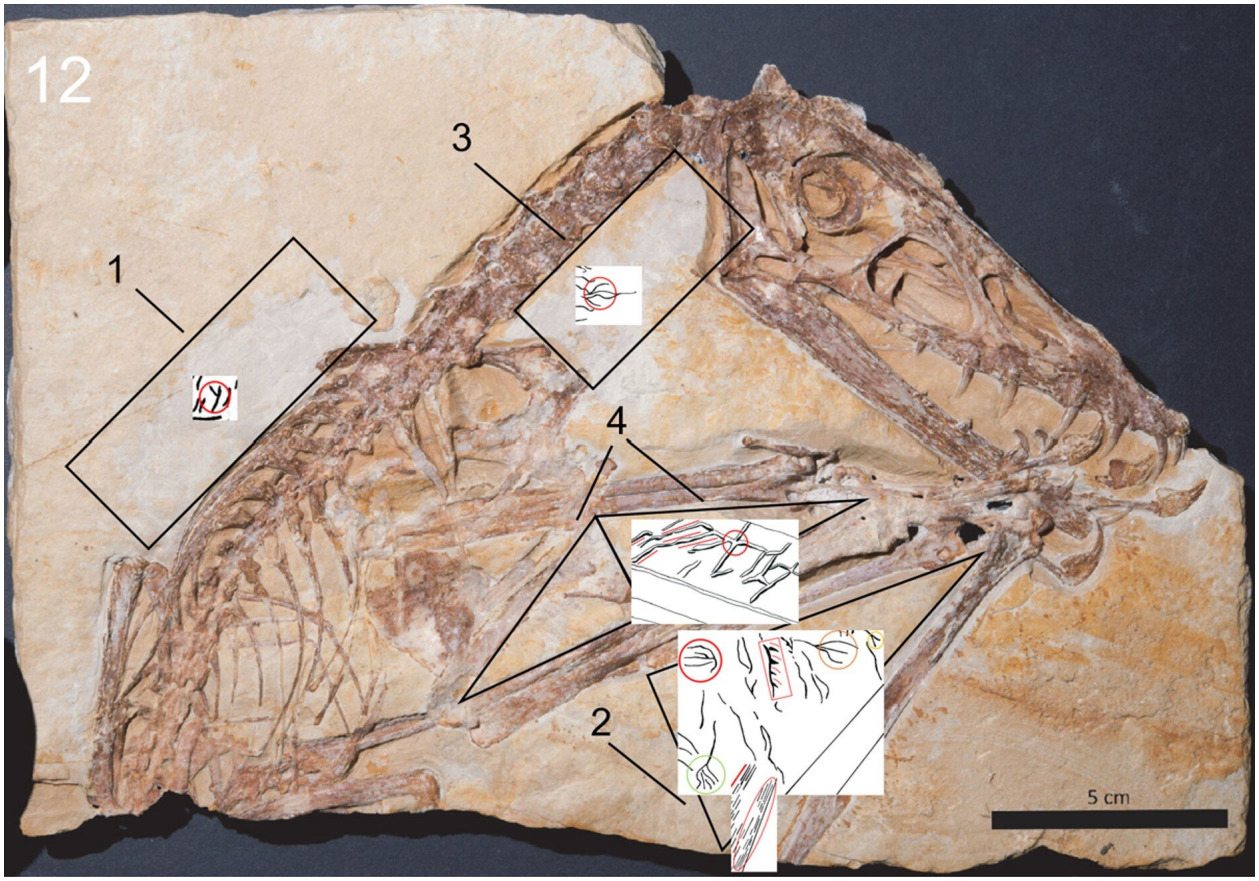

FIGURE 12. Distribution of the different soft tissue types occurring on the main slab of the *Scaphognathus crassirostris* holotype IGPB Goldfuß 1304a, illustrated in a modified version of Figure 2A. This Figure functions as a guide for the respective location of the soft part types intensively described in the manuscript and the captions to give an overview about their spatial distribution and their occurrence on the main slab, supported by the interpretative drawings of the soft tissues. Pycnofibre Type 2 (smaller red and yellow circles), Type 3 (orange circle), Type 4 (red rectangle), Type 5 (larger red circle), Type 6 (green circle), aktinofibrils (red ellipse), and putative patagium vessels marked by red transverse lines.

RTI images with their corresponding appearance under normal light. Furthermore, complementary methods can be used to visualise soft tissue preservation, e.g., UV (see Jäger et al., 2018). For object surfaces with a stronger relief, RTI is rather unsuitable. In this case, the use of supplementary methods, such as photogrammetry, can be a good way to study strongly three-dimensional surfaces.

Unusual Findings

Some extraordinary structures in the holotype of *Scaphognathus crassirostris* as well as some features of the surrounding rock surface require an additional note. Small pits in the region between the zeugopodial bones of both wings in the *Scaphognathus crassirostris* holotype (Figures 10C-10G and 11D-11G) seem to resemble those of the Dresden *Rhamphorhynchus* specimen SNSD-MMG BaJ 2210, which Wiman (1925) and Broili (1927) regarded as the remains of hair follicles, later confirmed for other specimens (Wellnhofer, 1975c). However, the pits in the holotype of *Scaphognathus crassirostris* are not associated with small grooves as in the Dresden specimen, suggesting that they might represent another organic structure (Broili, 1927; see illustration caption of Figure 10D and 10G for a detailed discussion). Instead of being organic in origin, there is also the possibility that these structures may have been formed taphonomically. In the Dresden *Rhamphorhynchus* specimen, these small pits and their associated fine grooves are not located on the actual wing membrane (Broili, 1927). This supports the idea that the corresponding structures in the *Scaphognathus crassirostris* holotype are not identical to the structures described by Broili (1927)

because, in the *Scaphognathus* specimen, the pits are restricted to the area of the former wing membrane. However, according to Wellnhofer (1975c), pits identical to the Dresden *Rhamphorhynchus* specimen are indeed part of the wing membrane in another *Rhamphorhynchus* specimen. Therefore, these small pits were in all probability not limited to the body alone, making an interpretation of their former organic composition and nature (i.e., hair follicles or other organic/inorganic structures) difficult.

Goldfuß (1831, p. 106f.) described the whitish amorphous rock surface containing pycnofibres next to the vertebral column (Figures 4A, 5D and 9A) as a “splittable, dissolved rock mass" and “very thin-slated". A similar preservation may also exist in *Germanodactylus rhamphastinus* (Wagner, 1851) (specimen number MCZ 1886), the holotype of *Pterorhynchus wellnhoferi* (CAGS02-IG-gausa-2/M 608), and the holotype of *Jeholopterus ningchengensis* (IVPP V12705). For the latter two, this surface was interpreted as remains of the epidermis or dermis (respectively), being closely associated with other pterosaurian soft tissue parts (Bennett, 2002; Kellner et al., 2010). Kellner et al. (2010) assumed that the epidermis or dermis in the holotype of *Jeholopterus ningchengensis* (IVPP V12705) might be preserved as phosphate, which likely also applies to the holotype of *Scaphognathus crassirostris*. Because epidermal structures are made up of keratin (Chatterjee and Templin, 2004; Schweitzer, 2011; Witton, 2013), the holotype of *Scaphognathus crassirostris* could support the keratinous composition for pycnofibres argued by Kellner et al. (2010).

Rounded, irregularly shaped, whitish stains between the zeugopodial bones of both wings (Figure 10A and 10B) are not identical with the whitish rock surface associated with the pycnofibres and are likely inorganic in origin. They might result from aqueous solutions resulting from the detachment of the uppermost rock layer (see caption of Figure 10B for discussion).

At least for pterosaurs from the Solnhofen area, the reddish colour of the bones of the *Scaphognathus crassirostris* holotype is rarely seen (Tischlinger, pers. comm., 2021). The reason for this colouration is unknown, but it could be associated with the precipitation of iron-rich minerals, which seem to have influenced almost all of the bone surface of the skeleton (see also Figure 10C).

Another unusual aspect is the line that extends along the phalanges of the right wing finger to the edge of the main and counter slab next to the aktinofibrils (Figure 9D-9F). It was previously mentioned by Goldfuß (1831) and interpreted as a remnant of a fold of the patagium or a muscle. Later, Wellnhofer (1975b) attributed this line to the wing membrane. Jäger et al. (2018) most recently interpreted this line as the border of the aktinopatagium. Two signs support the interpretation of Goldfuß that the patagium might have been folded in this area. The maximal distance of the line near the phalangeal articulation of the right wing finger is approximately 1.7 cm at the edge of both slabs. Therefore, the presumed edge of the patagium bordered by this line is narrower than generally assumed for the width of the wing membrane in this region (compare Bennett, 2000, figure 1, p. 256). Therefore, this piece of flight membrane might be derived from a section close to the trailing edge. Also, the bone surface of the first two phalanges is covered by slightly curved and discontinuously running elevations with a more or less parallel arrangement to each other. They cover most of the bone surface of the first two phalanges (see Figure 9D and 9E), at some places merging into each other. Due to their high similarity to the adjacent aktinofibril impressions, they are likely to also pertain to these structures.

Aktinofibril impressions on the bone surface can only be explained by a folding of the patagium over the phalanges. Bennett (2015) attributed comparable grooves in soft tissue impressions to the folding of the patagium. Thus, the distinctive line in the *Scaphognathus crassirostris* holotype might correspond to those in the famous “Zittel wing,” BSPG 1880 II 8 (Bennett, 2015).

Taphonomy

Goldfuß (1831) linked the formation of the pycnofibre impressions to the whitish amorphous rock surface associated with them (Figures 4A, 5D, and 9A), which is plausible in the context of the aforementioned preservation of the epidermis or dermis in this area in *Jeholopterus ningchengensis* (IVPP V12705) (Kellner et al., 2010). According to Goldfuß (1831, p. 107), lime layer deposits between the folded patagium and the integumentary appendages are said to have made the preservation of these soft tissues possible in the first place. The decomposition of the pterosaur carcass is also thought to have contributed to the formation of the white amorphous rock surfaces.

Due to the presence of the pycnofibre impressions as grooves on the main slab and as corresponding elevations on the counter slab (cf. Figure

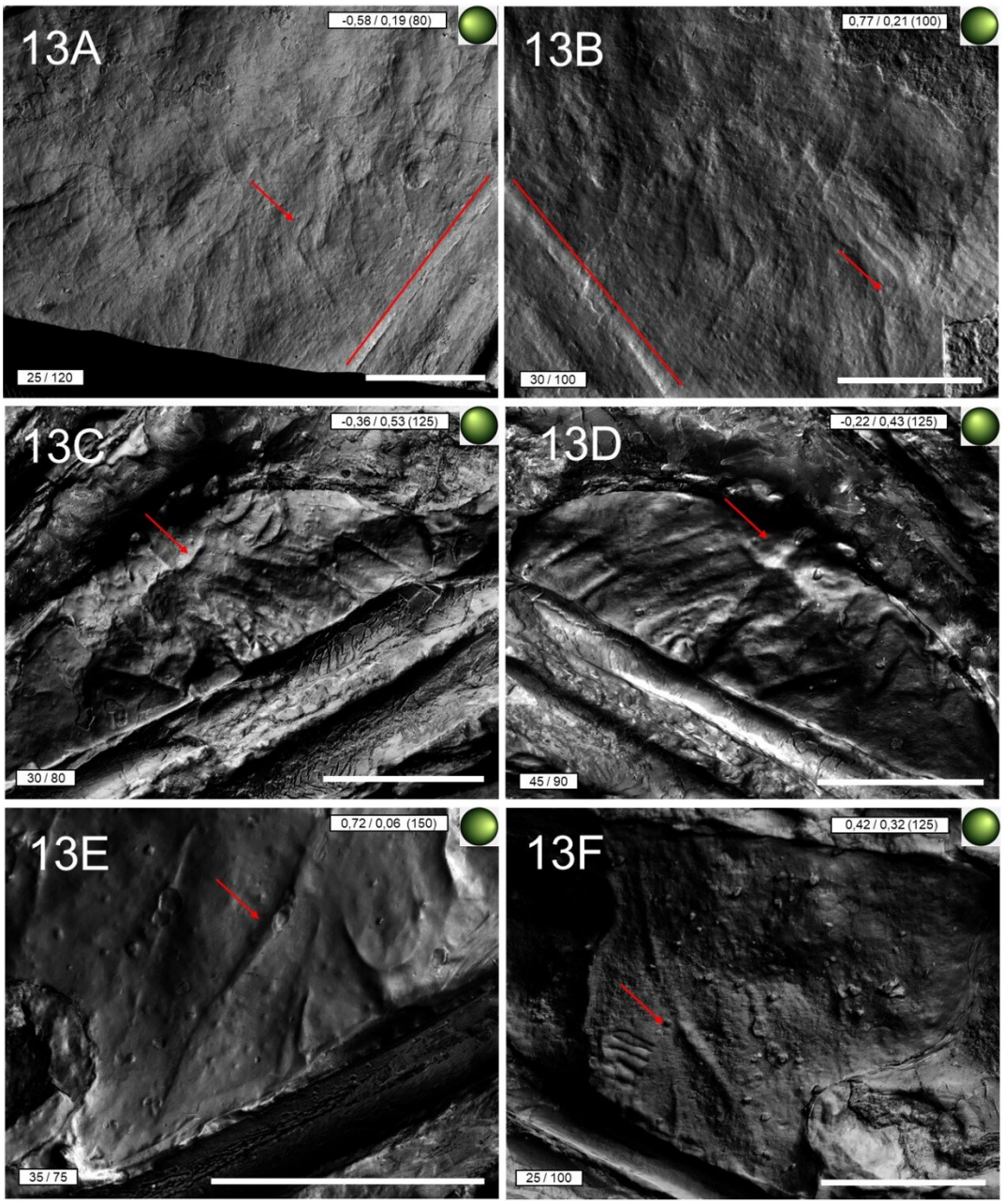

FIGURE 13. Different areas on the main slab as well as on the counter slab sum up the general mode of the soft part preservation in the *Scaphognathus crassirostris* holotype IGPB Goldfuß 1304b. The impressions on the main slab (images on the left figure side; 13A, 13C, and 13E) are in accordance with the corresponding elevations of the same impressions on the counter slab (right images 13B, 13D, and 13F; see for a direct comparison the red arrows). This illustrates the observation made by Goldfuß (1831), who stated that on the main slab, the soft part impressions are to be seen as grooves, whereas on the counter slab, they are shaped as elevations. This observation led Goldfuß (1831, p. 108) to the conclusion that the pycnofibres must have originally been under the limestone layer of the counter slab. **13A-13B.** Pycnofibre impressions and the remains of the wing membrane including the aktinofibrils close to the articulation of the first with the second phalanx of the right wing finger (putative patagium border marked in both images by a red transversal line). **13C-13D.** The impressions between the deltopectoral crest of the humerus and the zeugopodial bones of the right wing. Note the strong contrast between the deeply embedded grooves on the main slab (13C) and the clearly perceptible elevations on the counter slab (13D). **13E-13F.** Blood vessel impressions. The grooves of the blood vessels on the main slab trace the exact contour of the corresponding elevations on the counter slab.

13). Goldfuß concluded that the pycnofibres must have originally been under the limestone layer of the counter slab (Goldfuß, 1831, p. 108). This interpretation can also be applied to the other soft tissue types, i.e., the aktinofibrils and the vessels of the patagium. In general, Solnhofen Formation fossils are usually characterised by bones and soft tissues laying on the roof slab, whereas the impression of the fossil is present on the underlying slab (Viohl, 1994; Tischlinger and Frey, 2002).

Even in exceptionally preserved fossils, it is not easy to determine which surface features are derived from biological structures (i.e., those originally present in the living animal) and which are due to taphonomical influences. This is due to a variety of abiotic and biotic parameters influencing the morphology of the fossil (e.g., ontogeny, phylogeny, availability of oxygen, and the sediment in which burial took place; summarised in Sansom, 2014).

Therefore, the following discussion is split into two sections. The first focuses on possible taphonomic factors explaining the morphology of the apparent soft tissue impressions in the *Scaphognathus crassirostris* holotype. The purpose of this section is to highlight the importance of taphonomy and to question the assumption that the morphologies of the integumentary appendages in the fossil were the ones already present during the animal's lifetime. The second focuses on the biological influence of the preservation of potential anatomical structures in explaining the morphology of the pycnofibre types. For each pycnofibre type, we state which influence (biological vs. taphonomical) we prefer and why.

Biostratinomial transport could have affected the appearance of the integumentary structures in the *Scaphognathus crassirostris* holotype because movement of the carcass in the water column is assumed to be responsible for the disarticulation and loss of completeness of individual elements from the rest of the skeleton. Kellner et al. (2010) argued that pycnofibres were not attached strongly to the skin and might, therefore, have been lost and detached from the body easily, resulting in taphonomically displaced pycnofibre impressions no longer showing their original organisation and/or structure. Even before entering the water column, the lightly built skeletal anatomy of pterosaurs might have led to a prolonged residence time on the water surface with pycnofibres saturated in water, which can result in alteration to the structures of integumentary appendages (Kundrát, 2004; Foth, 2012; Beardmore et al., 2017). For example, as Kundrát (2004) pointed out, only a short period of water contact can produce an obscured feather morphology in which anatomical details fail to get preserved as impressions. However, the high degree of articulated skeletal elements and the extensive soft part preservation in the *Scaphognathus crassirostris* holotype, combined with the presence of phosphatic preservation, indicates a fast embedding of the carcass and a reducing environment (Wilson et al., 2016). This suggests that the carcass reached the bottom of the basin relatively undistorted and maybe immediately after death, though this conclusion should not exclude possible biostratinomial effects. Indeed, disturbing transport processes might not have lasted over an extended period of time, since it has been suggested that Solnhofen pterosaurs were strongly bound to their marginal-marine environment (Beardmore et al., 2017).

Moreover, bacterial mats may have been responsible for the formation of a protective sarcophagus, which might have enclosed the pterosaur carcass as a reasonable biological barrier against destructive taphonomical processes, favouring soft part preservation by precipitating biominerals such as calcium carbonate or calcium phosphate (Briggs and Kear, 1993; Iniesto et al., 2017). This sarcophagus might have given an advantage for the generation of impressions and furthermore acted as a preventive agent against disarticulation, as suggested by taphonomic experiments with recent anurans conducted by Iniesto et al. (2017).

However, some biostratinomial transport processes must have occurred in this specimen according to Tischlinger (2003, 2006). At least in some places, pycnofibres may have been washed together, potentially resulting in different pycnofibre types purely by chance, as it may have been the case for the alleged pycnofibre type of Figure 6D, E. These deposits of coincidentally arranged neighbouring integumentary appendages might simulate larger pycnofibre types that were never present in the living animal (see Feduccia et al., 2005). The pycnofibre impressions ventral to the zeugopodia of the right wing are likely to have been displaced because their location on the area of the former wing membrane seems unlikely according to newer models of the structure of the patagium (Tischlinger and Frey, 2002; Frey et al., 2003; Tischlinger, 2003, 2006; Kellner et al., 2010; Tischlinger and Frey, 2015, figure 917, p. 474). Therefore, Tischlinger (2003, 2006) assumed that the pycnofibre impressions close to the right wing

finger could have originated from pycnofibres from the ventral side of the animal.

It can be assumed that at least some of the branchings or crossings (especially Type 2, but also Type 3 pycnofibres) may have been formed due to taphonomy-related clumping of neighbouring integumentary appendages as a direct consequence of sedimentary compaction (Foth, 2012), though there is, at least in one case (the Type 3 impression ventral to the zeugopodia of the right wing), still the possibility of a distinct biological origin for the impression in question. Potential taphonomic factors to form such pycnofibre types may include overlapping of simple-shaped, non-branched integumentary appendages (Feduccia et al., 2005; Saitta et al., 2019) or the decomposition of the skin of the pterosaur carcass (Feduccia et al., 2005), but also objects placed between individual fibres (Lingham-Soliar, 2003; see p. 41). Clumping in turn may have resulted in artificial integumentary impressions sharing similarities with fossilised plumage known otherwise in the ornithodiran fossil record (e.g., Chen et al., 1998; Xu et al., 2001; Czerkas and Ji, 2002; Kellner et al., 2010; Godefroit et al., 2014; Yang et al., 2019). However, the “tuft” of the *Scaphognathus crassirostris* holotype specimen (Figure 6H) is marked by a much higher degree of symmetry and organisation, suggesting that it is more likely biological in origin.

Another possible example of taphonomical displacement during the biostratinomial phase might be the area dorsal to the dorsal vertebral column, for which a distinct change in the orientation of the pycnofibre tips can be documented (Figure 4). Feduccia et al. (2005) explain the different orientation of integumentary structures with a taphonomy-related re-arrangement of pieces (creasing, folding, overlying) of the skin and its decomposition.

In addition to the biostratinomy-related factors already mentioned, there may also be several diagenetic factors that might have affected the pterosaur carcass and the morphology of the former integumentary appendages. Diagenetic processes, such as high temperature and pressure, are essential factors when considering the preservation of biological structures (Saitta, 2015; Saitta et al., 2019). According to Saitta (2015), this diagenetic maturation can have major impacts on the morphology of integumentary appendages even at moderately low temperatures, resulting in a loss of crucial information (e.g., concerning their overall morphology).

Although taphonomic studies on ornithodiran integumentary appendages focus mainly on theropods (including modern-day birds, e.g., Foth, 2012; Saitta, 2015, Saitta et al., 2018, Saitta et al., 2019, Schweitzer et al., 2018; Zhao et al., 2020), their implications may also be applicable to pterosaurs, because general diagenetic processes such as compaction should likely have affected the morphology of the integumentary appendages independent from the phylogenetic position of the respective taxa. At the same time, potential limitations for direct comparisons between taphonomically induced variation in these structures should be considered, given the phylogenetic distance of pterosaurs relative to birds and their completely extinct status (see Sansom, 2014).

As exemplified by Foth (2012), diagenetic factors such as compaction can influence the shape of feathers of modern birds so they can no longer be distinguished from each other, for example due to compaction-induced overlapping of the plumage. Such a process could also have been the reason for the chaotic arrangement of many pycnofibre impressions in the holotype specimen of *Scaphognathus crassirostris*, in particular regarding the pycnofibre types ventral to the zeugopodia of the right wing (compare Figures 4D, 4E, 5A, 5B and 6A and 6C).

Therefore, the arrangement of the integumentary appendages itself as a densely packed plumage can complicate morphological interpretations (Saitta et al., 2019). Exceptionally fine details of integumentary appendages prone to decay and maturation-related changes can affect the overall morphology and, therefore, the morphological interpretation of the former structures, as suggested for example by Foth (2012), Saitta et al. (2017), Saitta et al. (2019) and Zhao et al. (2020). Furthermore, taphonomic experiments conducted by Saitta (2015) suggest that the degree of fusion of these anatomically fine details (such as barbs and barbules in recent bird feathers) might depend on whether other biostratinomial effects occurred prior to burial, such as a certain degree of decay. In sum, these factors should be considered as having affected at least some regions with integumentary appendages in the holotype specimen. These observations have implications for the interpretation of fossil integumentary appendages. In fact, the appearance of the integumentary appendages studied by Foth (2012) was comparable to the ones found in the fossil record of dinosaurs and pterosaurs, including the *Scaphognathus crassirostris* holotype (e.g., Chen et al., 1998; Xu et al.,

2001; Czerkas and Ji, 2002; Kellner et al., 2010; Godefroit et al., 2014; Yang et al., 2019; Zhang et al., 2008).

Furthermore, organic fibre types other than pycnofibres might have imitated the shape of some pycnofibre types described here. This refers above all to the aktinofibrils since it is not always easy to discriminate them from pycnofibres (Unwin and Martill, 2020). For example, fossilised and decomposed integumentary fibres may look quite similar in shape to pycnofibres and may have a variable organisation in the fossil record (cf. Lingham-Soliar, 2015, figure 6.1, p. 265). Morphologically, they can show great parallels to some of the pycnofibre impressions in the holotype, e.g., the second and sixth type (Figure 5A and 5B). According to Lingham-Soliar (2003), bifurcated structures such as Type 2 pycnofibres (Figures 5A-5B, 6G) could also be traced back to objects placed between individual integumentary fibres. These objects may have altered the appearance of the integumentary fibres before fossilisation, potentially leading to forked or feather-like structures (cf. Lingham-Soliar, 2003, figure 2a, p. 6) and superimposed fibres with different diameters might have resulted in feather-like impressions (cf. also Lingham-Soliar, 2003, figure 2b, p. 6).

Thence, it is important to emphasise that the shape of the pycnofibre impressions in the fossil record does not necessarily have to reflect the appearance of the integumentary appendages during the animal's lifetime. For that reason, most of the types described in this study should be treated with caution and not viewed as direct evidence for preserved anatomical structures, but more as the result of the combined influence of anatomical structures and taphonomical patterns.

However, there is the possibility that there are some regions on the main and counter slab where a biological signal is present. Saitta (2015) and Saitta et al. (2018) pointed out that interpretations of the integumentary appendages seen in the fossil record, especially in non-avian theropod dinosaurs (e.g., Chen et al., 1998; Xu et al., 2001; Zhang et al., 2008), might include structures with a partly preserved original integumental morphology. Referring to the *Scaphognathus crassirostris* holotype, the appearance of the two most complex pycnofibre types, i.e., the fifth and sixth one, might at least partly reflect the initial morphology they had prior to burial and diagenesis. Although the individual physicochemical parameters of the sedimentary environments of fossil deposits with exceptional fossil feather preservation were not accurately simulated, Saitta et al. (2018) emphasise the applicability of their experimentally gained results to the fossil record of Fossillagerstätten, which are hypothesised to be derived from low-energy aquatic sedimentary milieus (which is the case for the Solnhofen sedimentary basins). According to Saitta et al. (2018), even the permanent contact with water (in the case of submerged integumentary appendages) should not result in the clumping of anatomical feather traits leading to a loss of the finer morphological details, contra Foth (2012), making it possible that individual side branches in the holotype specimen might be preserved and are still describable.

Also, the early-compacted sediment surrounding the integumentary covering should act as a fixative for the position of individual integumentary structures (Saitta et al., 2018), arguing in the case of the *Scaphognathus crassirostris* specimen that especially in places where the pycnofibres were in close vicinity to the skeleton (e.g., dorsal to the dorsal vertebral column (see Figures 4 and 5), they might not be greatly displaced by early diagenetic processes like compaction. However, these conclusions should be treated with caution since at least in one place (ventral to the zeugopodia of the right wing), there is evidence for the taphonomical displacement of the pycnofibres.

However, the high degree of symmetry regarding the organisation of individual side branches makes it reasonable to assume that the more complex types, such as the Type 3 (Figure 6C-6E) or Type 5 (Figure 6H), are not (only) due to taphonomic factors, e.g., compaction or current activity in the Solnhofen sedimentary basin (see Saitta et al., 2019). For example, the three side branches of the Type 3 pycnofibre have approximately the same length and are almost symmetrically organised to each other (Figure 6F). And in the case of the Type 5 pycnofibre, there is an even increase in the length of the side branches from the outermost parts of the tuft towards the middle, difficult to explain by a coincidental taphonomically influenced arrangement of several individual pycnofibres washed together. In addition, the side branches of the tuft also have nearly the same distance to each other, which supports the view that in individual cases there is a well-founded suspicion of possible biological structures preserved in the holotype specimen. The assumption of an at least partly biologically influenced soft part preservation seems more likely because of reports on similar structures in other pterosaurs of varying taxonomic affinity and from other localities representing differ-

ent palaeoenvironmental, and therefore, taphonomical, settings (e.g., Yang et al., 2019). A tuft-like structure comparable to Type 5 in the *Scaphognathus crassirostris* holotype might also be present in the holotype of *Pterorhynchus wellnhoferi* (Czerkas and Ji, 2002).

It is plausible to assume that several different types of integumentary appendages were present on the body surface of pterosaurs, including simple monofilaments (comparable to Type 1), branched structures (Type 2), and tufts (Type 5), an assumption to which the studied holotype may contribute further evidence (see Benton et al., 2019). As Yang et al. (2020) pointed out, modern-day birds are characterised by distinct interspecific variation when it comes to feather morphologies and even a striking difference between closely related taxa concerning the existence or non-existence of these feather morphologies, so comparable variation in pterosaurs should not be considered unlikely.

Comparison with Other Pterosaur Finds

Pycnofibres. Due to the preservation of the soft parts as impressions, there is only a limited amount of information and therefore comparability with other pterosaurs, especially with regard to the complex interplay between different taphonomical factors affecting the appearance of the integumentary appendages. Hence, the focus of comparisons is on the observed preservational patterns, i.e., the pycnofibre types, in other pterosaurs relative to the *Scaphognathus crassirostris*. In general, these comparisons add new information to the comparability of pterosaurian soft part preservation, but in particular to some detailed considerations, such as that of Tischlinger (2003, 2006) concerning the detailed comparison between the preserved integumentary appendages of *Pterorhynchus wellnhoferi* and the *Scaphognathus crassirostris* holotype specimen. These comparisons are not claimed to be complete or to provide unequivocal evidence for the existence of certain anatomical traits, especially in the *Scaphognathus crassirostris* holotype. Another problem in the *Scaphognathus crassirostris* holotype that should not be neglected is the very limited, often only singular occurrence of certain types as in the case of the tuft (type 5) or the feather (type 6), so that no reliable statements can be made about the former occurrence (including their spatial distribution) of certain pycnofibre types, which also limits the detailed comparison (above all in terms of their respective frequency) of similar pycnofibre types occurring in our specimen and others (see Figure 12).

The observed soft tissues and associated structures are in accordance with those of other pterosaurs from the Solnhofen Formation (e.g., Broili, 1927; Frey and Martill, 1998; Tischlinger and Frey, 2002; Frey et al., 2003; Tischlinger and Frey, 2015). This is especially true for the pycnofibres. For example, several specimens of the genus *Rhamphorhynchus* show clear signs of an extensive pycnofibre coverage, including the Dresden specimen SNSD-MMG BaJ 2210 described by Wanderer (1908). That specimen shows an association of tiny pit-like holes with fine grooves of short length, particularly in the triangle formed by the humerus and the zeugopodial bones of the right wing. Broili (1927) assumed that these holes could be interpreted as the remains of hair follicles. Corresponding structures might also exist in the *Scaphognathus crassirostris* holotype in the same region (Figures 10C, 10D, 10G, and 11E- 11G; see subchapter 4.3; unusual findings), but with a slightly different appearance of the tiny pits compared to the Dresden specimen (see above).

Following the description of Broili (1927), the putative pycnofibre impressions of the Dresden *Rhamphorhynchus* specimen resemble the ones of the *Scaphognathus crassirostris* holotype: curved, with recognisable overlaps as well as a different orientation relative to the vertebral column and depending on the body region (Figure 4C-4E). Such hair-like pycnofibres are also known from several pterodactyloids from the Solnhofen Formation, indicating pycnofibres of variable length and spatial arrangement, e.g., in tufts (e.g., Frey and Martill, 1998; Vidovic and Martill, 2014). In particular, the pycnofibres of *Pterodactylus micronyx* (*Aurorazhdarcho micronyx* sensu Bennett, 2013; specimen ELTE V 256) have a surprising similarity with the Type 1 impressions dorsal to the dorsal vertebral column in the *Scaphognathus crassirostris* holotype (see Tischlinger and Frey, 2015, figure 913, p. 473; see also Figure 4C). Tufts and unbranched, simple impressions likely resembling Type 1 and Type 5 are also known from the holotype of *Jeholopterus ningchengensis* (IVPP V12705; Figures 6H, 7C) and from other pterosaurs from the northeastern Chinese Tiaojishan Formation and the Solnhofen Formation, e.g., *Pterorhynchus wellnhoferi* Czerkas and Ji, 2002, *Pterodactylus kochi* (Wagner, 1837), and various Chinese anurognathids (Frey and Martill, 1998; Czerkas and Ji, 2002; Wang et al., 2002; Kellner et al., 2010; Yang et al., 2019). Czerkas and Ji (2002,

p. 4), for example, mention that in *Pterorhynchus wellnhoferi* "individual filaments appear to spread from a single follicle" and their point of origin can be described as a short basis, similar to Type 5 in the *Scaphognathus crassirostris* holotype (Figure 6H). Whereas Type 1 and Type 5 pycnofibre impressions found in the *Scaphognathus crassirostris* holotype might be applicable to other pterosaur finds, others might be either much less distributed among other pterosaur taxa or were not present in the living animal at all. First and foremost, this refers to the bifurcated Type 2, the trident-shaped Type 3, and Type 4 with side branches only observable at one side of the main branch. Although even more complex-branched types have been described in other pterosaurs (see Yang et al., 2019), none of those described for anurognathids perfectly accords with the pycnofibre types observed using RTI in the *Scaphognathus crassirostris* holotype. Even with regard to the most complex pycnofibre Type 6 (the feather-like pycnofibre impression), there seems to be a corresponding structure in the *Pterorhynchus wellnhoferi* holotype, which, according to Tischlinger (2003, 2006), bears a striking similarity with an ostrich feather (a term also used by Goldfuß to describe a feather-like structure in the *Scaphognathus crassirostris* holotype).

Aktinofibrils and presumed wing membrane of the aktinopatagium. The aktinofibrils were not mentioned by Goldfuß (1831) in his original description. This is most likely due to their low visibility when observed with the naked eye.

The few aktinofibril impressions neither allow reliable conclusions about their former density in the aktinopatagium nor their organic composition. Although UV imaging increases their visibility (Jäger et al., 2018; Figures 8D-8E), it is not possible to determine the former composition of organic material based on UV images (Lingham-Soliar, 2015). The preserved aktinofibril impressions suggest no radiating pattern, as is known from other pterosaurs from the Solnhofen Formation, e.g., the Zittel wing (BSPG 1880 II 8; see Bennett, 2000, 2015; Tischlinger and Frey, 2002; Kellner et al., 2010). Instead, the few aktinofibril impressions preserved indicate a closely spaced and almost parallel arrangement (see Figure 9E-9F). Furthermore, there is no evidence for the presence of several aktinofibril layers with different orientations to each other, as is known from the holotype of *Jeholopterus ningchengensis* (IVPP V12705; Kellner et al., 2010). The appearance of the impressions does not preclude the assumption that aktinofibrils were made up of a relatively resistant material such as keratin, as hypothesised by several authors (Padian and Rayner, 1993a, 1993b; Bennett, 2000; Tischlinger and Frey, 2002; Chatterjee and Templin, 2004; Witton, 2013; Bennett, 2015).

Despite their supposed small diameter of only 0.05-0.2 mm (Wellnhofer, 1975c; Padian and Rayner, 1993a; Bennett, 2015; Hone et al., 2015), aktinofibrils left fine but clear impressions. Moreover, they are the only remains of the aktinopatagium that resisted decay long enough to produce clear impressions, suggesting that they were among the last organic components of the wing to be decayed, probably related to their keratinous composition (Bennett, 2015). The fact that there is evidence (including the completeness of the bones forming the leading edge of the wing as well as the preservation of the actual membrane itself) that the patagium as a whole was resistant to decay (Beardmore et al., 2017) suggests the same for its component structures.

However, such parallel-running, exceptionally fine and longitudinal impressions observed in the *Scaphognathus crassirostris* holotype (compare Figure 9D-9E) also show a certain similarity with non-pterosaurian Mesozoic marine reptiles, i.e., ichthyosaurs (Lingham-Soliar, 1999, fig. 2; Lingham-Soliar and Plodowski, 2007, fig. 2h) and mosasaurs (compare Lindgren et al., 2010, fig. 6c; Lindgren et al., 2011, fig. 1b; Lindgren et al., 2013, fig. 3d), in which these soft tissue traces are derived from collagenous connective and dermal tissues. For this reason, the holotype does not provide unambiguous evidence for the former organic composition of the aktinofibrils as keratinous. If the sharply defined line along the phalanges of the right wing finger is interpreted as part of the aktinopatagium (Jäger et al., 2018), the aktinofibrils found outside of this line must have been transported taphonomically, maybe during the decay stage of the pterosaur wing membrane. Diagenetic influence on the position of the aktinofibrils has also been considered for other Solnhofen pterosaurs (e.g., Tischlinger and Frey, 2002).

The patagium section containing the aktinofibrils impressions may not have belonged to the trailing edge of the wing membrane due to the lack of intercalations (cf. Figure 8E). In this area, the aktinofibrils normally show intercalations with each other (Wellnhofer, 1991; Bennett, 2015), i.e., an insertion of an aktinofibril within the space formed by two adjacent aktinofibrils. The absence of intercalating aktinofibrils is also evidence for why this section must have been located at a greater dis-

tance from the trailing edge of the wing (Wellnhofer, 1987; Bennett, 2000; Tischlinger and Frey, 2002; Frey et al., 2003; Chatterjee and Templin, 2004; Kellner et al., 2010; Witton, 2013; Bennett, 2015; Hone et al., 2015).

However, it cannot be completely excluded that the patagium was folded after the death of the animal, making it difficult to speculate about the exact position of the wing membrane section. Suggested by the comparison with other pterosaur finds, e.g., the Zittel wing (cf. Wellnhofer, 1987, figure 3, p. 156, Wellnhofer, 1991, p. 152; Padian and Rayner, 1993a, figure 4E, p. 113), the parallel arrangement of the aktinofibrils with respect to the phalanges of the right wing finger leads to the conclusion that this section of the wing membrane already must have been located near the wing finger in the living animal.

Blood vessels and suspected wing membrane of the tenopatagium. The blood vessels distal to the deltopectoral crest of the humerus (see Figure 10F-10G) can only partly be compared with the complex vessel system in the *Rhamphorhynchus* specimen JME SOS 4784 described by Tischlinger and Frey (2002) and Frey et al. (2003). Due to their arrangement at regular distances to each other and their moderate curvature, the blood vessels in the holotype specimen might be comparable to the main branches forking from the most prominent vessel in JME SOS 4784 (illustration caption of Figures 10F and 11A). In JME SOS 4784, these tubes are said to show a bifurcation in the direction of the trailing edge of the brachiopatagium (Frey et al., 2003). The distal ends of the tubes are themselves connected with arc-shaped tubes and have medially and laterally originating smaller bifurcations. If the vessels in the *Scaphognathus crassirostris* holotype are identical to those described by Frey et al. (2003), then the preservation of the former ventral blood vessel layer supposed to have existed according to newer models of the pterosaur wing (e.g., Tischlinger and Frey, 2002) would be very modest. An interesting difference between this specimen and JME SOS 4784 is the prominent bifurcation of the rightmost vessel, resembling an inverted “Y” (Figure 10). However, the most prominent vessel and the smaller bifurcations originating from the main side branches described in JME SOS 4784 cannot be detected in the area distal to the deltopectoral crest of the humerus in the *Scaphognathus crassirostris* holotype. However, the thickest blood vessel in Figure 10F and 10G is similar in diameter to the main vessel in JME SOS 4784. If recent models of the structure of the patagium are correct, these blood vessels would be part of the ventral side of the multi-layered wing membrane (Tischlinger and Frey, 2002; Frey et al., 2003; Bennett, 2015; Tokita, 2015).

Small pits directly associated with the blood vessels might be the result of degradation processes in the context of the taphonomy of the pterosaur carcass (Figure 10F) or might be linked with the pycnofibres and their preservation. Comparable structures might be present in some specimens of the genus *Rhamphorhynchus*, including the Dresden specimen SNSD-MMG BaJ 2210, where these pits show an irregular distribution comparable to the *Scaphognathus crassirostris* holotype (Broili, 1927). However, the specular enhancement images cannot confirm the existence of fine grooves between the pits in the *Scaphognathus crassirostris* holotype, which are present in SNSD-MMG BaJ 2210. In this *Rhamphorhynchus* specimen, these fine grooves were assumed to have been derived from original organic structures due to their association with these pits (Broili, 1927).

Due to their limited occurrence in the area of the former patagium (compare Figures 10A-10D and 11A-11D), it is highly probable that the grooves proximal to the deltopectoral crest of the humerus of the right wing are either the remains of the wing membrane or are their taphonomic products. Their variable length, visibility, and orientation indicate that they might represent another vessel type but may not be blood vessels like the ones distal to the deltopectoral crest of the humerus. They do not have the same moderate curvature as the blood vessels, nor do they have bifurcations in the same manner as them. Moreover, they are characterised by a distinct length difference between the longest main groove and the other half-sized grooves, which are only roughly half the length of the main groove (compare red markings in Figure 10B-10D). Such a distinct length difference is not present in the blood vessels distal to the deltopectoral crest of the humerus or for the main branches forking from the most prominent vessel in JME SOS 4784 (the tubular structures with a brighter central canal in JME SOS 4784). However, it is possible that the most prominent, i.e., the longest groove proximal to the deltopectoral crest of the humerus might be the counterpart of the tubular structures described in JME SOS 4784. Besides, the vessels in the *Scaphognathus crassirostris* holotype proximal to the deltopectoral crest of the humerus share the same parallel arrangement with the thinner tubes branching off at regular distances from the main

vessel as described for JME SOS 4784 (Tischlinger and Frey, 2002; Frey et al., 2003). Therefore, it cannot be ruled out that both structures–proximal and distal to the deltopectoral crest of the humerus —represent blood vessels, and that their mode of preservation might be different between the two regions. Apart from the blood vessel layer, none of the other tissue layers (i.e., the fibre and fascia layer) described for JME SOS 4784 bears similarity with the soft tissues near the deltopectoral crest in the *Scaphognathus crassirostris* holotype (Tischlinger and Frey, 2002; Frey et al., 2003). Despite Jäger et al. (2018) having interpreted them as pycnofibres, the organisation of these putative vessels also compares well with the vessel system of JME SOS 4784, suggesting that they are true remains of the patagium and not those of the body coverage. No aktinofibrils are present in the entire area between the zeugopodia of both wings. This supports the hypothesis that this section of the former wing membrane may have belonged to the tenopatagium (cf. Unwin and Bakhurina, 1994; Bennett, 2000, figure 1, p. 256; Kellner et al., 2010; Witton, 2013).

CONCLUSIONS

The publication of Georg August Goldfuß from 1831 contained the first life reconstruction of an extinct vertebrate to be based on a detailed scientific description, including soft part impressions and their interpretation as body coverage in the holotype of the Late Jurassic pterosaur *Scaphognathus crassirostris*.

With the help of an optical imaging technique called reflectance transformation imaging (RTI), six different and partly undescribed pycnofibre types could be detected: unbranched (1), bifurcations (2), trident-shaped (3), a type similar to the first one but with side branches pointing caudally (4), tuft (5), and feather-like (6). These and similar findings from other pterosaurs from the Solnhofen Formation and from the northeastern Chinese Tiaojishan Formation support the postulate of a body coverage in pterosaurs composed of several pycnofibre types, (e.g., Frey and Martill, 1998; Yang et al., 2019). Discrepancies with the observations of Goldfuß are mainly in the position of individual soft part impressions and their interpretation, but also in soft part types not described by Goldfuß, e.g., the aktinofibrils of the aktinopatagium (Jäger et al., 2018). Both aktinofibrils and blood vessels demonstrate the existence of at least two different layers in the patagium (Tischlinger and Frey, 2002; Frey et al., 2003). However, the exact location of the wing membrane section and the comparability of the vessels with other pterosaurian finds coming from the Solnhofen Formation is difficult to determine.

However, the similarity of some pycnofibre types, particularly with respect to Type 1, with comparable structures described in the context of the preservation of other biological fibre types in taxa unrelated to pterosaurs, e.g., ichthyosaurs, might also suggest an important influence of the Solnhofen basin taphonomy on the pterosaur carcass (Lingham-Soliar, 2003; Tischlinger, 2003, 2006; Foth, 2012). Nevertheless, other pycnofibre types, such as Types 5 and 6, resemble the description of comparable structures in other pterosaur specimens to such a high degree (e.g., Czerkas and Ji, 2002) that they might indicate a widespread occurrence of specific pycnofibre types in pterosaurs of varying taxonomic affinity and from different palaeoenvironmental settings.

ACKNOWLEDGEMENTS

NH thanks co-author KJ and G. Oleschinski for the introduction to RTI and support for making the RTI images and both KJ and PMS for proofreading, which contributed to a much higher quality of this paper. NH also would like to thank the Handling Editor CK for corrections and commentaries, which also greatly improved this publication.

REFERENCES

Andres, B., Clark, J.M., and Xing, X. 2010. A new rhamphorhynchid pterosaur from the Upper Jurassic of Xinjiang, China, and the phylogenetic relationships of basal pterosaurs. Journal of Vertebrate Paleontology, 30:163-187. https://doi.org/10.1080/02724630903409220

Barbosa, J.G., Sobral, J.L., and Proença, A.J. 2007. Imaging techniques to simplify the PTM generation of a bas-relief, p. 28-31. In Ioannides, M., Arnold, D.B., Niccolucci, F., and Mania, K. (eds.), The 7th International Symposium on Virtual Reality, Archaeology and Intelligent Cultural Heritage (VAST 2006). Eurographics Association, Nicosia.

Barthel, K.W. 1964. Zur Entstehung der Solnhofener Plattenkalke (unteres Untertithon). Mitteilungen der Bayerischen Staatssammlung für Paläontologie und historische Geologie, 4:37-69.

Barthel, K.W. 1970. On the deposition of the Solnhofen lithographic limestone (Lower Tithonian, Bavaria, Germany). Neues Jahrbuch für Geologie und Paläontologie Abhandlungen, 135(1):1-18.

Barthel, K.W., Swinburne, N.H.M., and Morris, S.C. 1990. Solnhofen: A Study in Mesozoic Palaeontology. Cambridge University Press, Cambridge. https://doi.org/10.1086/417353

Beardmore, S.R., Lawlor, E., and Hone, D.W.E. 2017. Using taphonomy to infer differences in soft tissues between taxa: an example using basal and derived forms of Solnhofen pterosaurs. The Science of Nature, 104:65. https://doi.org/10.1007/s00114-017-1486-0

Bennett, S.C. 2000. Pterosaur flight: The role of actinofibrils in wing function. Historical Biology, 14:255-284. https://doi.org/10.1080/10292380009380572

Bennett, S.C. 2002. Soft tissue preservation of the cranial crest of the pterosaur *Germanodactylus* from Solnhofen. Journal of Vertebrate Paleontology, 22:43-48.

Bennett, S.C. 2007. A second specimen of the pterosaur *Anurognathus ammoni.* Paläontologische Zeitschrift, 81:376-398. https://doi.org/10.1007/bf02990250

Bennett, S.C. 2013. New information on body size and cranial display structures of *Pterodactylus antiquus*, with a revision of the genus. Paläontologische Zeitschrift, 87:269-289. https://doi.org/10.1007/s12542-012-0159-8

Bennett, S.C. 2014. A new specimen of the pterosaur Scaphognathus crassirostris, with comments on constraint of cervical vertebrae number in pterosaurs. Neues Jahrbuch für Geologie und Paläontologie Abhandlungen, 271:327-348. https://doi.org/10.1127/0077-7749/2014/0392

Bennett, S.C. 2015. New interpretation of the wings of the pterosaur *Rhamphorhynchus muensteri* based on the Zittel and Marsh specimens. Journal of Paleontology, 89:845-869. https://doi.org/10.1017/jpa.2015.68

Benton, M.J. and Pfretzschner, H.U. 2007. Paläontologie der Wirbeltiere (Third Edition). Dr. Friedrich Pfeil, München, Germany.

Benton, M.J., Dhouailly, D., Jiang, B., and McNamara, M. 2019. The Early Origin of Feathers. Trends in Ecology & Evolution, 34:856-869. https://doi.org/10.1016/j.tree.2019.04.018

Béthoux, O., Llamosi, A., and Toussaint, S. 2016. Reinvestigation of *Protelytron permianum* (Insecta; Early Permian; USA) as an example for applying reflectance transformation imaging to insect imprint fossils. Fossil Record, 20(1):1-7. https://doi.org/10.5194/fr-20-1-2016

Briggs, D.E.G. and Kear, A.J. 1993. Fossilization of soft tissue in the laboratory. Science, 259:1439-1442. https://doi.org/10.1126/science.259.5100.1439

Broili, F. 1927. Ein *Rhamphorhynchus* mit Spuren von Haarbedeckung. Sitzungsberichte der Bayerischen Akademie der Wissenschaften, Mathematisch-Naturwissenschaftliche Abteilung, 1927:49-67.

Broili, F. 1938. Beobachtungen an *Pterodactylus*. Sitzungberichte der Bayerischen Akademie der Wissenschaften, Mathematisch-Naturwissenschaftliche Abteilung, 1938:139-154.

Broili, F. 1939. Ein *Dorygnathus* mit Hautresten. Sitzungsberichte der Bayerischen Akademie der Wissenschaften, Mathematisch-Naturwissenschaftliche Abteilung, 1939(6):128-134.

Caine, M. and Magen, M. 2011. Pixels and Parchment: The Application of RTI and Infrared Imaging to the Dead Sea Scrolls. Electronic Visualisation and the Arts:140-146.

Carpenter, K., Unwin, D.M., Cloward, K., Miles, C., and Miles, C. 2003. A new scaphognathine pterosaur from the Upper Jurassic Morrison Formation of Wyoming, USA. Geological Society of London, London, Special Publications, 217:45-54. https://doi.org/10.1144/gsl.sp.2003.217.01.04

Chatterjee, S. and Templin, R.J. 2004. Posture, locomotion, and paleoecology of pterosaurs (Vol. 376). Geological Society of America, Boulder, 376: 1–64. https://doi.org/10.1130/0-8137-2376-0.1

Chen, P.J., Dong, Z.M., and Zhen, S.N. 1998. An exceptionally well-preserved theropod dinosaur from the Yixian Formation of China. Nature, 391:147-152. https://doi.org/10.1038/34356

Cheng, X., Wang, X., Jiang, S., and Kellner, A.W.A. 2012. A new scaphognathid pterosaur from western Liaoning, China. Historical Biology, 24:101-111. https://doi.org/10.1080/08912963.2011.635423

Colbert, E.H. 1969. A Jurassic Pterosaur from Cuba. American Museum Novitates, 2370:1-26.

Collini, C.A. 1784. Sur quelques Zoolithes du Cabinet d'Histoire naturelle de S. A. S. E. Palatine & de Bavière, à Mannheim. Acta Academiae Theodoro-Palatinae, 5:58-103.

Cosentino, A. 2013. Macro photography for reflectance transformation imaging. E-conservation Journal, 1:71-85. https://doi.org/10.18236/econs1.201310

Cuvier, G. 1809. Mémoire sur le squelette fossile d'un reptile volant des environs d'Aichstedt, que quelques naturalistes ont pris pour un oiseau, et dont nous formons un genre de Sauriens, sous le nom de Ptero-Dactyle. Annales du Muséum national d'Histoire Naturelle, Paris, 13:424-437.

Czerkas, S.A. and Ji, Q. 2002. A new rhamphorhynchoid with a headcrest and complex integumentary structures. Feathered Dinosaurs and the Origin of Flight, 1:15-41.

Döderlein, L. 1923. *Anurognathus ammoni*, ein neuer Flugsaurier. Sitzungsberichte der Mathematisch-Physikalischen Klasse der Bayerischen Akademie der Wissenschaften, 1923:117-164.

Duffy, S.M. 2010. Polynomial texture mapping at Roughting Linn rock art site, p. 213-217. In Proceedings of the ISPRS Commission V Mid-Term Symposium: Close Range Image Measurement Techniques. ISPRS Commission, Newcastle upon Tyne.

Earl, G., Martinez, K., and Malzbender, T. 2010. Archaeological applications of polynomial texture mapping: analysis, conservation and representation. Journal of Archaeological Science, 37:2040-2050. https://doi.org/10.1016/j.jas.2010.03.009

Elgin, R.A., Hone, D.W.E., and Frey, E. 2011. The extent of the pterosaur flight membrane. Acta Palaeontologica Polonica, 56(1):99-111. https://doi.org/10.4202/app.2009.0145

Feduccia, A., Lingham-Soliar, T., and Hinchliffe, J.R. 2005. Do feathered dinosaurs exist? Testing the hypothesis on neontological and paleontological evidence. Journal of Morphology, 266:125-166. https://doi.org/10.1002/jmor.10382

Foth, C. 2012. On the identification of feather structures in stem-line representatives of birds: evidence from fossils and actuopalaeontology. Paläontologische Zeitschrift, 86:91-102. https://doi.org/10.1007/s12542-011-0111-3

Frey, E. and Martill, D.M. 1998. Soft tissue preservation in a specimen of *Pterodactylus kochi* (Wagner) from the Upper Jurassic of Germany. Neues Jahrbuch für Geologie und Paläontologie Abhandlungen, 210:421-441. https://doi.org/10.1127/njgpa/210/1998/421

Frey, E., Meyer, C.A., and Tischlinger, H. 2011. The oldest azhdarchoid pterosaur from the Late Jurassic Solnhofen Limestone (Early Tithonian) of Southern Germany. Swiss Journal of Geosciences, 104:35-55. https://doi.org/10.1007/s00015-011-0073-1

Frey, E., Tischlinger, H., Buchy, M.-C., and Martill, D.M. 2003. New specimens of Pterosauria (Reptilia) with soft parts with implications for pterosaurian anatomy and locomotion. Geological Society, London, Special Publications, 217:233-266. https://doi.org/10.1144/GSL.SP.2003.217.01.14

Gasparini, Z., Fernández, M., and Fuente, M. de la. 2004. A new pterosaur from the Jurassic of Cuba. Palaeontology, 47:919-927. https://doi.org/10.1111/j.0031-0239.2004.00399.x

Godefroit, P., Sinitsa, S.M., Dhouailly, D., Bolotsky, Y.L., Sizov, A.V., McNamara, M.E., Benton, M.J., and Spagna, P. 2014. A Jurassic ornithischian dinosaur from Siberia with both feathers and scales. Neues Jahrbuch für Geologie und Paläontologie Abhandlungen, 345:451-455. https://doi.org/10.1126/science.1253351

Goldfuß, G.A. 1831. Beiträge zur Kenntnis verschiedener Reptilien der Vorwelt. Nova Acta Physico-Medica Academiae Caesareae Leopoldino-Carolinae Naturae Curiosorum, 15:61-128.

Hammer, Ø. and Spocova, J. 2013. Virtual whitening of fossils using polynomial texture mapping. Palaeontologia Electronica, 16:1-10. https://doi.org/10.26879/384

Hammer, Ø., Bengtson, S., Malzbender, T., and Gelb, D. 2002. Imaging fossils using reflectance transformation and interactive manipulation of virtual light sources. Palaeontologia Electronica, 4:1-9. https://palaeo-electronica.org/2002_1/fossils/issue1_02.htm

He, X., Yan, D., and Su, D. 1983. A new pterosaur from the middle Jurassic of Dashanpu, Zigong, Sichuan. Journal of Chengdu College, Geology, Supplement, 1:27-33.

Hone, D.W.E., Henderson, D.M., Therrien, F., and Habib, M.B. 2015. A specimen of *Rhamphorhynchus* with soft tissue preservation, stomach contents and a putative coprolite. PeerJ, 3:e1191. https://doi.org/10.7717/peerj.1191

Iniesto, M., Villalba, I., Buscalioni, A.D., Guerrero, M.C., and López-Archilla, A.I. 2017. The effect of microbial mats in the decay of anurans with implications for understanding taphonomic processes in the fossil record. Scientific Reports, 7:1-12. https://doi.org/10.1038/srep45160

Jäger, K.R.K., Tischlinger, H., Oleschinski, G., and Sander, P.M. 2018. Goldfuß was right: Soft part preservation in the Late Jurassic pterosaur *Scaphognathus crassirostris* revealed by reflectance transformation imaging and ultraviolet light and the auspicious beginnings of paleo-art. Palaeontologia Electronica, 21(3):1-20. https://doi.org/10.26879/713

Kellner, A.W.A., Wang, X., Tischlinger, H., de Almeida Campos, D., Hone, D.W.E., and Meng, X. 2010. The soft tissue of *Jeholopterus* (Pterosauria, Anurognathidae, Batrachognathinae) and the structure of the pterosaur wing membrane. Proceedings of the Royal Society B: Biological Sciences, 277:321-329. https://doi.org/10.1098/rspb.2009.0846

Keupp, H. 1993. Aspects of the origin of the Solnhofen lithographic limestone facies based on a new core drilling in the Maxberg Quarry. Geobios, 27:71-80. https://doi.org/10.1016/s0016-6995(94)80022-7

Kölbl-Ebert, M. and Cooper, B.J. 2019. Solnhofener Plattenkalk: a heritage stone of international significance from Germany. Geological Society, London, Special Publications, 486(1):103-113. https://doi.org/10.1144/sp486-2017-324

Kundrát, M. 2004. When did theropods become feathered? – Evidence for pre-*Archaeopteryx* feathery appendages. Journal of Experimental Zoology Part B: Molecular and Developmental Evolution, 302:355-364. https://doi.org/10.1002/jez.b.20014

Lindgren, J., Caldwell, M.W., Konishi, T., and Chiappe, L.M. 2010. Convergent evolution in aquatic tetrapods: insights from an exceptional fossil mosasaur. PloS ONE, 5:e11998. https://doi.org/10.1371/journal.pone.0011998

Lindgren, J., Everhart, M.J., and Caldwell, M.W. 2011. Three-dimensionally preserved integument reveals hydrodynamic adaptations in the extinct marine lizard *Ectenosaurus* (Reptilia, Mosasauridae). PLoS ONE, 6:e27343. https://doi.org/10.1371/journal.pone.0027343

Lindgren, J., Kaddumi, H.F., and Polcyn, M.J. 2013. Soft tissue preservation in a fossil marine lizard with a bilobed tail fin. Nature Communications, 4:2423. https://doi.org/10.1038/ncomms3423

Lingham-Soliar, T. 1999. Rare soft tissue preservation showing fibrous structures in an ichthyosaur from the Lower Lias (Jurassic) of England. Proceedings of the Royal Society of London. B: Biological Sciences, 266:2367-2373. https://doi.org/10.1098/rspb.1999.0933

Lingham-Soliar, T. 2003. Evolution of birds: ichthyosaur integumental fibers conform to dromaeosaur protofeathers. Naturwissenschaften, 90:428-432. https://doi.org/10.1007/s00114-003-0448-x

Lingham-Soliar, T. 2015. The Vertebrate Integument Volume 2: Structure, Design and Function. Springer, Berlin Heidelberg. https://doi.org/10.1007/978-3-662-46005-4

Lingham-Soliar, T. and Plodowski, G. 2007. Taphonomic evidence for high-speed adapted fins in thunniform ichthyosaurs. Naturwissenschaften, 94:65-70. https://doi.org/10.1007/s00114-006-0160-8

Longrich, N.R., Martill, D.M., and Andres, B. 2018. Late Maastrichtian pterosaurs from North Africa and mass extinction of Pterosauria at the Cretaceous-Paleogene boundary. PLOS Biology, 16(3):e2001663. https://doi.org/10.1371/journal.pbio.2001663

Lu, J.C., Fucha, X.H., and Chen, J.M. 2010. A new scaphognathine pterosaur from the Middle Jurassic of western Liaoning, China. Diqiu Xuebao (Acta Geoscientica Sinica), 31:263-266.

Lü J., Unwin, D.M., Zhao, B., Gao, C., and Shen, C. 2012. A new rhamphorhynchid (Pterosauria: Rhamphorhynchidae) from the Middle/Upper Jurassic of Qinglong, Hebei Province, China. Zootaxa, 3158:1-19. https://doi.org/10.11646/zootaxa.3158.1.1

MacDonald, L.W. 2011. Visualising an Egyptian Artefact in 3D: Comparing RTI with Laser Scanning. Electronic Visualisation and the Arts:155-162.

Malzbender, T., Gelb, D., Wolters, H., and Zuckermann, B. 2000. Enhancement of Shape Perception by Surface Reflectance Transformation. Hewlett-Packard Technical Report, HPL-2000-38, March 2000. Hewlett-Packard Company, Palo Alto.

Malzbender, T., Gelb, D., and Wolters, H. 2001. Polynomial texture maps, p. 519-528. In Pocock, L. (ed.), Proceedings of ACM SIGGRAPH. ACM, New York, USA. https://doi.org/10.1145/383259.383320

Mayr, G., Pittman, M., Saitta, E., Kaye, T.G., and Vinther, J. 2016. Structure and homology of *Psittacosaurus* tail bristles. Palaeontology, 59:793-802. https://doi.org/10.1111/pala.12257

Meyer, v.H. 1846. *Pterodactylus* (*Rhamphorhynchus*) *Gemmingi* aus dem Kalkschiefer von Solenhofen. Palaeontographica, 1:1-20.

Monninger, S., Frey, E., and Tischlinger, H. 2012. Supporting structures in the flight membrane of pterosaurs. 10th Annual Meeting of the European Association of Vertebrate Paleontologists, 20:165-168.

Mudge, M., Malzbender, T., Schroer, C., and Lum, M. 2006. New reflection transformation imaging methods for rock art and multiple-viewpoint display, p. 195-202. In Ioannides, M., Arnold, D.B., Niccolucci, F., and Mania, K. (eds.), The 7th International Symposium on Virtual Reality, Archaeology and Intelligent Cultural Heritage (VAST 2006). Eurographics Association, Nicosia.

Padian, K. and Rayner, J.M.V. 1993a. The wings of pterosaurs. American Journal of Science, 293(A):91-166. https://doi.org/10.2475/ajs.293.a.91

Padian, K. and Rayner, J.M.V. 1993b. Structural fibers of the pterosaur wing: anatomy and aerodynamics. Naturwissenschaften, 80:361-364. https://doi.org/10.1007/bf01138791

Rauhut, O.W.M., López-Arbarello, A., Röper, M., and Rothgaenger, M. 2017. Vertebrate fossils from the Kimmeridgian of Brunn: the oldest fauna from the Solnhofen Archipelago (Late Jurassic, Bavaria, Germany). Zitteliana, 89:305-329.

Reisdorf, A.G. and Wuttke, M. 2012. Re-evaluating Moodie's opisthotonic-posture hypothesis in fossil vertebrates Part I: Reptiles—the taphonomy of the bipedal dinosaurs *Compsognathus longipes* and *Juravenator starki* from the Solnhofen Archipelago (Jurassic, Germany). Palaeobiodiversity and Palaeoenvironments, 92:119-168. https://doi.org/10.1007/s12549-011-0068-y

Saitta, E.T. 2015. The taphonomy of keratin in archosaurs. Published Thesis, School of Earth Sciences, University of Bristol, Bristol, UK.

Saitta, E.T. 2018. The Taphonomy of Soft Tissues and the Evolution of Feathers. PhD Thesis. University of Bristol, Bristol, UK.

Saitta, E.T., Clapham, C., and Vinther, J. 2018. Experimental subaqueous burial of a bird carcass and compaction of plumage. Paläontologische Zeitschrift, 92:727-732. https://doi.org/10.1007/s12542-018-0411-y

Saitta, E.T., Kaye, T.G., and Vinther, J. 2019. Sediment-encased maturation: a novel method for simulating diagenesis in organic fossil preservation. Palaeontology, 62:135-150. https://doi.org/10.1111/pala.12386

Saitta, E.T., Rogers, C.S., Brooker, R.A., and Vinther, J., 2017. Experimental taphonomy of keratin: a structural analysis of early taphonomic changes. PALAIOS, 32:647-657. https://doi.org/10.2110/palo.2017.051

Sansom, R.S. 2014. Experimental decay of soft tissues. The Paleontological Society Papers, 20: 259-274. https://doi.org/10.1017/s1089332600002886

Schaller, D. 1985. Wing evolution, p. 333-348. In Hecht, M.K., Ostrom, J.H., Viohl, G., and Wellnhofer, P. (eds.), Proceedings of the International *Archaeopteryx* Conference, Eichstätt 1984. Freunde des Jura-Museums Eichstätt, Eichstätt.

Schweitzer, M.H. 2011. Soft tissue preservation in terrestrial Mesozoic vertebrates. Annual Review of Earth and Planetary Sciences, 39:187-216. https://doi.org/10.1146/annurev-earth-040610-133502

Schweitzer, M.H., Zheng, W., Moyer, A.E., Sjövall, P., and Lindgren, J. 2018. Preservation potential of keratin in deep time. PloS ONE, 13:1-17. https://doi.org/10.1371/journal.pone.0206569

Sträng, K.A. 2009. Efficient flapping flight of pterosaurs. Stanford University, Stanford, California, USA.

Tischlinger, H. 2003. Professor Goldfuß und sein "Dickschnabel" aus dem Altmühljura. Globulus Beiträge der Natur- und kulturwissenschaftlichen Gesellschaft, 10:95-104.

Tischlinger, H. 2006. … und Goldfuß hatte doch Recht! Fossilien, 23:245-253.

Tischlinger, H. and Frey, E. 2002. Ein *Rhamphorhynchus* (Pterosauria, Reptilia) mit ungewöhnlicher Flughauterhaltung aus dem Solnhofener Plattenkalk. *Archaeopteryx*, 20:1-20.

Tischlinger, H. and Frey, E. 2013. Ein neuer Pterosaurier mit Mosaikmerkmalen basaler und pterodactyloider Pterosauria aus dem Ober-Kimmeridgium von Painten (Oberpfalz, Deutschland). *Archaeopteryx*, 31:1-13.

Tischlinger, H. and Frey, E. 2015. Flugsaurier (Pterosauria), p. 459-480. In Arratia, G., Schultze, H.-P., Tischlinger, H., and Viohl, G. (eds.), Solnhofen – Ein Fenster in die Jurazeit. Dr. Friedrich Pfeil, München, Germany.

Tokita, M. 2015. How the pterosaur got its wings. Biological Reviews of the Cambridge Philosophical Society, 90:1163-1178. https://doi.org/10.1111/brv.12150

Unwin, D.M. and Bakhurina, N.N. 1994. *Sordes pilosus* and the nature of the pterosaur flight apparatus. Nature, 371:62-64. https://doi.org/10.1038/371062a0

Unwin, D.M. and Martill, D.M. 2020. No protofeathers on pterosaurs. Nature Ecology & Evolution, 4:1590-1591. https://doi.org/10.1038/s41559-020-01308-9

Vidovic, S.U. and Martill, D.M. 2014. *Pterodactylus scolopaciceps* Meyer, 1860 (Pterosauria, Pterodactyloidea) from the Upper Jurassic of Bavaria, Germany: the problem of cryptic pterosaur taxa in early ontogeny. PloS ONE, 9(10):e110646. https://doi.org/10.1371/journal.pone.0110646

Viohl, G. 1990. Taphonomy of Fossil-Lagerstätten. Solnhofen Lithographic Limestones, p. 285-289. In Briggs, D.E.G. and Crowther, P.R. (eds.), Palaeobiology. A synthesis. Blackwell, Oxford, UK.

Viohl, G. 1994. Fish taphonomy of the Solnhofen Plattenkalk – an approach to the reconstruction of the palaeoenvironment. Geobios, 27:81-90. https://doi.org/10.1016/S0016-6995(94)80023-5

Wagner, J.A. 1837. Beschreibung eines neuentdeckten *Ornithocephalus*: nebst allgemeinen Bemerkungen über die Organisation dieser Gattung. Abhandlungen der Bayerischen Akademie der Wissenschaften, Mathematisch-Naturwissenschaftliche Klasse, 2:165-198.

Wagner, J.A. 1851. Beschreibung einer neuen Art von *Ornithocephalus* etc. Abhandlungen der Bayerischen Akademie der Wissenschaften, Mathematisch-Physikalische Klasse, 6:127-192.

Wagner, J.A. 1859. Über einige, im lithographischen Schiefer neu aufgefundene Schildkröten und Saurier. Bulletin der königlichen Bayerischen Akademie der Wissenschaften, 22:554-555.

Wagner, J.A. 1860. Bemerkungen über die Arten von Fischen und Sauriern, welche im untern wie im oberen Lias zugleich vorkommen sollen. Sitzungsberichte der königlichen Bayerischen Akademie der Wissenschaften, Mathematisch-Physikalische Klasse, 1860:36-52.

Wagner, J.A. 1861. Uebersicht über die fossilen Reptilien des lithographischen Schiefers in Bayern nach ihren Gattungen und Arten. Sitzungsberichte der königlich Bayerischen Akademie der Wissenschaften zu München, 1861:497-535.

Wanderer, K. 1908. *Rhamphorhynchus Gemmingi* H. v. Meyer. Palaeontographica (1846-1933):195-216.

Wang, X., Zhou, Z., Zhang, F., and Xu, X. 2002. A nearly completely articulated rhamphorhynchoid pterosaur with exceptionally well-preserved wing membranes and “hairs” from Inner Mongolia, northeast China. Chinese Science Bulletin, 47:226-230.

Wellnhofer, P. 1975a. Die Rhamphorhynchoidea (Pterosauria) der Oberjura-Plattenkalke Süddeutschlands. Teil I. Allgemeine Skelettmorphologie. Paläontographica A, 148:1-33.

Wellnhofer, P. 1975b. Die Rhamphorhynchoidea (Pterosauria) der Oberjura-Plattenkalke Süddeutschlands. Teil II. Systematische beschreibung. Paläontographica A, 148:132-186.

Wellnhofer, P. 1975c. Die Rhamphorhynchoidea (Pterosauria) der Oberjura-Plattenkalke Süddeutschlands. Teil III. Palökologie und Stammesgeschichte. Paläontographica A, 149:1-30.

Wellnhofer, P. 1987. Die Flughaut von *Pterodactylus* (Reptilia, Pterosauria) am Beispiel des Wiener Exemplares von *Pterodactylus kochi* (Wagner). Annalen des Naturhistorischen Museums in Wien. Serie A für Mineralogie und Petrographie, Geologie und Paläontologie, Anthropologie und Prähistorie, 88:149-162.

Wellnhofer, P. 1991. The Illustrated Encyclopedia of Pterosaurs. Crescent Books, New York, USA.

Wellnhofer, P. 2008. A short history of pterosaur research. Zitteliana: B28: 7-19.

Wilson, P., Parry, L.A., Vinther, J., and Edgecombe, G.D. 2016. Unveiling biases in soft tissue phosphatization: extensive preservation of musculature in the Cretaceous (Cenomanian) polychaete *Rollinschaeta myoplena* (Annelida: Amphinomidae). Palaeontology, 59:463-479. https://doi.org/10.1111/pala.12237

Wiman, C. 1925. Über *Pterodactylus westmani* und andere Flugsaurier. Bulletin of the Geological Institute of the University of Upsala, 20:1-38.

Witton, M.P. 2013. Pterosaurs. Natural History, Evolution, Anatomy. Princeton University Press, Princeton, USA. https://doi.org/10.1515/9781400847655

Xu, X., Zhou, Z.H., and Prum, R.O. 2001. Branched integumental structures in *Sinornithosaurus* and the origin of feathers. Nature, 410:200-204. https://doi.org/10.1038/35065589

Yang, Z., Jiang, B., McNamara, M.E., Kearns, S.L., Pittman, M., Kaye, T.G., Orr, P.J., Xu, X., and Benton, M.J. 2019. Pterosaur integumentary structures with complex feather-like branching. Nature Ecology & Evolution, 3:24-30. https://doi.org/10.1038/s41559-018-0728-7

Yang, Z., Jiang, B., McNamara, M.E., Kearns, S.L., Pittman, M., Kaye, T.G., Orr, P.J., Xu, X., and Benton, M.J. 2020. Reply to: No protofeathers on pterosaurs. Nature Ecology & Evolution, 4:1592-1593. https://doi.org/10.1038/s41559-020-01309-8

Young, C.-C. 1964. On a new pterosaurian from Sinkiang, China. Vertebrata PalAsiatica, 8:221-255.

Zhao, T., Hu, J., Hu, L., and Pan, Y. 2020. Experimental maturation of feathers: implications for interpretations of fossil feathers. Palaios, 35:67-76. https://doi.org/10.1098/rsbl.2013.0184

Zhang, F., Zhou, Z., Xu, X., Wang, X., and Sullivan, C. 2008. A bizarre Jurassic maniraptoran from China with elongate ribbon-like feathers. Nature, 455:1105-1108. https://doi.org/10.1038/nature07447

Zhou, C.F. 2014. Cranial morphology of a *Scaphognathus*-like pterosaur, *Jianchangnathus robustus*, based on a new fossil from the Tiaojishan Formation of western Liaoning, China. Journal of Vertebrate Paleontology, 34:597-605. https://doi.org/10.1080/02724634.2013.812100

Zhou, C.F. and Schoch, R.R. 2011. New material of the non-pterodactyloid pterosaur *Changchengopterus pani* Lü, 2009 from the Late Jurassic Tiaojishan Formation of western Liaoning. Neues Jahrbuch für Geologie und Paläontologie Abhandlungen, 260:265-275. https://doi.org/10.1127/0077-7749/2011/0131

Zittel, K.A. 1882. Über Flugsaurier aus dem lithographischen Schiefer Bayerns. Palaeontographica, 29:47-80.